The Institute of Paper Chemistry

Appleton, Wisconsin

Doctor's Dissertation

The Determination of the Energy Site Distribution of the Surface of Cellulose Fibers by Gas Adsorption Methods

Harry A. Barber

January, 1969

THE DETERMINATION OF THE ENERGY SITE DISTRIBUTION OF THE SURFACE OF CELLULOSE FIBERS BY GAS ADSORPTION METHODS

A thesis submitted by

Harry A. Barber

B.S. 1964, State University of New York College of Forestry at Syracuse University
M.S. 1966, Lawrence University

in partial fulfillment of the requirements of The Institute of Paper Chemistry for the degree of Doctor of Philosophy from Lawrence University, Appleton, Wisconsin

January, 1969

TABLE OF CONTENTS

SUMMARY

Previous investigations of the physical adsorption of gases on the cellulose surface have been primarily concerned with obtaining either B.E.T. surface areas or pore size distributions of the samples in question. None of the previous investigations dealt with the determination of the energy site distribution of the adsorbent from gas adsorption isotherms.

In the present work, isotherms were determined volumetrically for the physical adsorption of argon gas on a variety of cellulosic surfaces at one or two temperatures. Certain noncellulosic adsorbents were also employed to broaden the range of low adsorptive potential samples studied.

From argon adsorption isotherms on a solvent-exchanged and dried purified cotton cellulose at 77.5 and 90.1°K, the applicability of Ross and Olivier Case 1 analysis was confirmed. Experimental and theoretical isosteric heats of adsorption were in good agreement as were calculated and observed values of the mean adsorptive potential.

The cellulose surface was characterized as exhibiting a very wide range of adsorptive potentials. The value of the mean adsorptive potential was observed to be quite low.

Solvent exchange and drying, and humidification and drying procedures were used to develop varying surface areas in a cotton cellulose sample. The dependence of the determined Ross and Olivier energy site distribution on available sample surface area was shown to be minor.

Several chemically modified cellulose samples were prepared to investigate the effects of modification on the determined energy site distribution. Periodate oxidation resulted in only very minor changes in the obtained distribution while both hydroxyethylation and the presence of hemicelluloses lowered the value of the mean adsorptive potential.

For all samples studied, marked discrepancies were observed between B.E.T. and Ross and Olivier estimates of surface area. Ross and Olivier surface area estimates were from 2.25 to 3.97 times the corresponding B.E.T. area estimates. Geometric surface areas determined for normal viscose rayon, high-tenacity viscose rayon, and the anatase form of titanium dioxide were considerably greater than the corresponding B.E.T. areas. It was concluded that the B.E.T. theory produced surface area estimates that were grossly in error. Ross and Olivier area estimates were in all cases greater than the corresponding geometric area estimates.

The relative correctness of the B.E.T. area estimate was shown to be dependent on the mean adsorptive potential of the sample.

Calculations showed that almost two-thirds of the cellulose surface possessed adsorptive potentials less than that of liquid argon. Therefore, beyond a surface coverage of about 0.3, the already adsorbed argon presented a more favorable adsorptive site than the remaining bare cellulose surface. Significant multilayer build-up occurred on the more energetic patches of the surface while the lower energy patches remained sparsely occupied, even at high equilibrium pressures.

It was shown that the B.E.T. theory is not valid for obtaining surface area estimates for samples exhibiting low mean adsorptive potentials and heterogeneous energy site distributions (e.g., the anatase form of titanium dioxide, cellulose, silver iodide, teflon 6, diamond dust). "Low mean adsorptive potentials" may be considered present if a significant part of the surface exhibits adsorptive potentials less than that of the liquid adsorbate. The construction of a linear B.E.T. plot from adsorption data was shown to be an insufficient criterion for obtaining valid surface area estimates.

Finally, the Ross and Olivier method of obtaining an energy site distribution from an adsorption isotherm was shown to be superior to the method of Adamson and Ling. The Ross and Olivier method required neither an independent (B.E.T.) estimate of monolayer capacity, nor a step function approximation, both of which are necessary for the method of Adamson and Ling.

Results of this study should be of value for the determination of surface area, bonded area, and bond strength values of pulp and paper samples.

INTRODUCTION

The nature of a solid surface differs from that of a liquid surface in that the surface molecules are not mobile at ordinary temperatures. Unlike a liquid, a solid is unable to rearrange its surface molecules to achieve an equipotential surface of minimum free energy. The presence of crystal faces, edges, corners, and other structural arrangements are certain to create a variation of surface energy from one location on the solid surface to another. One would also expect the affinity of a solid surface for foreign atoms to be a function of both the topography and stereochemistry of the surface. Knowledge of the character of this energy variation over the surface would probably be of importance in the investigation of certain phenomena such as catalysis, wetting, and adsorption.

Characterization of the energy site distribution of the surface of cellulose fibers may well prove useful in the investigation of related areas such as fiber-fiber bond strength, dye retention, coating adhesion, swelling, surface area determinations, etc.

HISTORICAL REVIEW

GAS ADSORPTION ON CELLULOSE

The physical adsorption of gas on cellulose samples is a method that has been used rather extensively in investigations concerned with characterization of the cellulose fiber surface. Fiber surface areas and pore size distributions were generally the quantities sought after by most of the investigators (1).

The gas adsorption theory of Brunauer, Emmett, and Teller (2) has received the widest acceptance for the determination of the surface area of cellulose samples from gas adsorption data (1). Pore size distributions for cellulose adsorbents have most frequently been determined using the Pierce method (3).

Relatively few examinations of the thermodynamics of gas adsorption on cellulose have been carried out (4, 5). Rowen and Blaine (5) determined free energies of adsorption for nitrogen on cotton as a function of partial pressure while Haselton (4) computed both free energies and isosteric heats of adsorption as a function of surface coverage for nitrogen and butane on a variety of cellulosic adsorbents. Clark (6) speculated as to the possibility of using gas adsorption as a tool to investigate the energy site distribution of the surface of cellulose fibers. With direct reference to the decreasing differential heats of adsorption for nitrogen on cellulose reported by Haselton (4), Clark felt that the cellulose surface should, therefore, possess a rather broad range of adsorptive potentials. However, this idea was not investigated further at that time.

DETERMINATION OF ENERGY SITE DISTRIBUTIONS FROM GAS ADSORPTION ISOTHERMS

ANALYTICAL SOLUTIONS

In recent years, several methods have been proposed for the determination of the distribution of adsorptive potentials on a solid surface from gas adsorption data.

From the overall isotherm equation, the fraction covered

$$\Theta(p,T) = \int_0^\infty \theta_i(p,T,U_{oi})\phi(U_o)dU_o \qquad (1)$$

where $\theta_i(p,T,U_{oi})$ represents a local isotherm function and $\phi(U_o)$ represents the energy site distribution function, one may obtain $\phi(U_o)$ in a number of ways. In the above equation,

p = pressure, mm. Hg

T = absolute temperature

U_o = adsorptive potential, defined as the difference in potential energy of a molecule in its lowest energy state in a gas and its zero point vibrational level in the adsorbed phase on the surface

U_{oi} = the midpoint value of adsorptive potential for the ith patch

Drain and Morrison (7) differentiated Equation (1) to obtain

$$\phi(U_o) = \frac{1}{\Theta}\frac{d\Theta}{dU_o} \, . \qquad (2)$$

They then substituted for θ_i in Equation (2) according to

$$\theta_i(p,U_o) = \begin{cases} 0, U_o < U_{oi}(p,T) \\ 1, U_o > U_{oi}(p,T) \end{cases} \qquad (3)$$

and obtained

$$\phi(U_o) = \frac{d\Theta}{dU_o} \text{ as } T \rightarrow 0. \tag{4}$$

However, as Ross (8) pointed out, to meet the experimental requirements for the condition outlined in Equation (3), very strenuous experimental efforts were necessary. The method required that both heats of adsorption and heat capacities of the adsorbed film be measured at a series of low temperatures as a function of surface concentration, thereby permitting the determination of the zero degree heats of adsorption by extrapolation. At absolute zero, the differential heat of adsorption q^{diff} is defined by

$$q^{diff} = U_o + {}_aP^{ia} \tag{5}$$

where ${}_aP^{ia}$ represents the lateral interaction term to account for lateral attractions among adsorbed molecules. Ross and Olivier (9) observed that the lateral interaction term was not computed by Drain and Morrison (7) and regarded this as a drawback to an otherwise elegant method. Due to the rigors of the required experimental conditions, this method has been used correctly only once by Drain and Morrison for the adsorption of oxygen and nitrogen on rutile.

Other workers have attempted to make use of Equation (2) by merely differentiating the isosteric heat curve which was obtained at temperatures considerably above absolute zero. Chessick and Zettlemoyer (10) attempted to obtain a distribution of the acid strengths of exchange sites on attapulgite clay from measurements of the heat of wetting in butylamine. They used differential heat values obtained at 25°C. rather than absolute zero and thereby introduced an unknown amount of uncertainty in their derived distribution, since vibrational motions of the adsorbed molecules were included in the energy terms. Young and Healey (11) attempted to obtain energy site distribution curves for the adsorption of argon on both activated and unactivated Chrysotile asbestos at -195°C. and -183°C. Like Chessick and Zettlemoyer (10), they also applied Equation (2) without making the necessary measurements and thereby introduced an unknown amount of uncertainty into the distributions which they obtained.

Several other attempts have been made to achieve an analytical solution of Equation (1). Halsey and Taylor in Ross (8) proposed an exponential distribution of sites according to

$$f_i = C' \exp^{(-U_o/U_o')} \qquad (6)$$

where U_o represented the energy difference between the lowest energy state of the gas and the lowest energy state of the adsorbed complex and C a constant. U_o' represented the mean of this difference. They also chose the Langmuir equation for θ_i in Equation (1), thereby introducing the limitation of localized adsorption without lateral interaction for the adsorbed phase. Integration of Equation (1) over all values of U_o, both positive and negative, yielded the Freundlich isotherm equation.

Sips (12) proposed an alternative method for the solution of Equation (1). By assuming functions for both the adsorption isotherm $\Theta(p)$ and the local isotherm $\theta(p,U_o)$, it was possible to derive the distribution function $\phi(U_o)$. Sips chose an empirical equation for $\Theta(p)$ and the Langmuir equation for $\theta(p,U_o)$ and demonstrated that a unique solution existed for $\phi(U_o)$. Again, the implication of localized adsorption without lateral interaction was the basis of the model. This type of approach implied severe restrictions on the mathematical form of the isotherm. Honig and Reyerson (13) have criticized Sips' failure to consider the important lateral interaction term.

In an effort to avoid the restrictions of the Langmuir model, Harkins and Stearns (14) attempted to characterize mobile adsorption with lateral interaction on a heterogeneous surface. Simplifications necessary to allow for derivation of their explicit local isotherm function effectively destroyed their model as was pointed out by Ross and Olivier (9). The authors themselves admitted that their equation had no physical basis and that the equation resulted from a desire to solve explicitly for θ_i. It was the opinion of Ross and Olivier (9) that the solution of Equation (1) is probably not possible for models of localized or mobile adsorption when both lateral interaction and surface heterogeneity are considered.

NONANALYTICAL SOLUTIONS

To avoid restrictions introduced by either the Langmuir equation or by undesirable simplifications necessary for an analytical solution of Equation (1), a few attempts have been made to achieve a nonanalytical solution.

Adamson and Ling (15) developed a method whereby the site energy distribution $\phi(U_o)$ may be obtained from an experimental adsorption isotherm $\Theta(p,T)$ and an arbitrarily assumed local isotherm function, θ_i. Since their method was graphical, it was not necessary to introduce either Θ or θ analytically, and successive approximations were used. The authors chose either the Langmuir equation or the Langmuir equation with lateral interaction term for θ_i. Experimental Θ values were calculated using B.E.T. theory monolayer capacity determinations. Site energy distributions for the adsorption of butane, argon, and nitrogen were reported.

Ross and Olivier (9) employed a nonideal two-dimensional van der Waals' equation of state for θ and assumed a Gaussian distribution of adsorptive energies for $\phi(U_o)$. They then computed a number of model isotherms using various values of the parameters involved. The final energy site distributions were obtained by comparing the computed isotherms with the experimental isotherms. The method provided for its own determination of V_β, the monolayer capacity. The use of a two-dimensional van der Waals' equation was based on the experimental findings of Ross and Winkler (17) that an adsorbed gas film was mobile and of the two-dimensional nonideal type. The adsorption model provided for lateral interactions in the adsorbed phase. Obtained distributions were temperature invariant, and the model correctly predicted adsorption behavior at various temperatures for a number of adsorption systems. Gregg and Sing (16) reviewed the theory of Ross and Olivier with general approval. They questioned, however, the divergence of B.E.T. and Ross and Olivier area estimates for rutile and diamond dust, noting that these estimates had been in fair agreement for a large number of other higher potential adsorbents.

Hsieh (18) studied the adsorption of argon on carbon black (MT-3100) and employed the Adamson and Ling method to obtain the energy site distribution at 77.8°K. The obtained distribution was Gaussian-like, very similar to that assumed by Ross and Olivier (9). He felt that the agreement was striking despite the difference in the local isotherm function assumed [i.e., the Langmuir isotherm in his work and the van der Waals' equation of state in Ross's work (17)]. Hsieh concluded that the method of Adamson and Ling (19) was rather insensitive to the isotherm selected and that any local isotherm function θ may be chosen without giving an entirely different distribution curve. This conclusion was further substantiated by observations of Ross (8) on the work of Hobson (20). In a later paper Adamson and Ling (19) presented evidence toward the more far-reaching conclusion that there is generally less uncertainty as to the distribution of heterogeneities than as to the type of adsorption model being obeyed (i.e., that the former characterization dominated the latter).

Hobson (20) has recently modified the Polanyi potential theory to permit the determination of an energy site distribution from an adsorption isotherm without having to make assumptions as to the shape of the distribution. This method does not consider adsorption to proceed by filling the consituent patches in serial order of their adsorptive energies. The local isotherm was assumed to follow one of three isotherm equations, all of which may be inverted so that a computer was not necessary for this method. Ross (8) has reviewed the method of Hobson in some detail. He pointed out that Hobson's adsorption potential, E', has been defined arbitrarily and also is not temperature invariant. The relationship of the thermodynamic heat of adsorption to the parameter E' has been defined so that it is not possible to predict temperature dependencies for the adsorption model. To use Hobson's method, a prior estimate of the monolayer capacity must be obtained.

ANALYSIS OF THE PROBLEM

EXPECTED ADSORPTION CHARACTERISTICS FOR A CELLULOSE-INERT GAS SYSTEM

The cellulose polymer is a spatial array of several types of atoms and functional groups which separately or in combination would be expected to exhibit a relatively wide range of forces of attraction to an adsorbate molecule. In addition, both the fringed fibril and the fringed micelle theories for the structure of cellulose consider the solid to be composed of high order and low order regions. Surface irregularities such as crystal corners, edges, faces, and those of the amorphous region are present in abundance. Such irregularities would be expected to produce variations in the magnitude of dispersion forces, which would be the predominant forces in the cellulose-inert gas system (9).

The above considerations of both the chemical and physical nature of cellulose would lead to the hypothesis that the cellulose surface would be expected to exhibit a relatively broad range of adsorptive potentials.

The application of Graham's (21) equilibrium function is useful in characterizing the type of adsorption occurring in a given system. Graham defined the equilibrium function, Z, by

$$Z = \frac{R}{(1-R)(D)} \tag{7}$$

where R represents the degree of monolayer completion, and D equals the relative saturation pressure (P/P_o). For the case of adsorption without lateral interaction on a homogeneous surface, a plot of Z versus R yielded a straight line parallel to the R axis. Adsorption with lateral interaction was characterized by an increasing Z value after a portion of the surface had been covered. Adsorption on a heterogeneous surface with lateral interaction was indicated by an initial decrease of the Z value followed by a leveling off of the curve. Graham has emphasized that this function is only useful to gain insight as to the type of adsorption occurring in a given system and that it is not possible to obtain quantitative estimates of the degree of surface heterogeneity through its application.

Values of Graham's equilibrium function were calculated from the data of Haselton (4) for the adsorption of nitrogen on chlorite holocellulose at 77.5°K. These values showed the adsorption system could be classified as heterogeneous with lateral interaction.

This classification of adsorption immediately rules out the possibility of making use of any of the analytical methods of obtaining an energy site distribution for cellulose.

The theory of Ross and Olivier (9) was chosen as the one best suited for the determination of the energy site distribution of cellulose. This theory permits an independent determination of V_β, the monolayer capacity, while both Hobson's (20) and Adamson and Ling's (15) methods require B.E.T. determinations of that quantity. Estimates of the Ross and Olivier monolayer capacity, V_β, at two different temperatures were in good agreement for a number of adsorbants, while the temperature variation of B.E.T. v_m estimates is a common criticism of that theory (16). It is the opinion of Gregg and Sing (16) that the applicability of the Ross and Olivier theory to the low pressure region of the isotherm (below 0.05 p/p_o) is an important improvement over the B.E.T. theory which frequently is not suitable at low pressures. The model of Ross and Olivier (9) is the only model of the three discussed that is both complete thermodynamically and that yields distributions that are temperature invariant.

The model of Ross and Olivier is also the only model compatible with the concept of a mobile adsorbed film. Ross and Pultz (22) studied the adsorption of argon and nitrogen on both boron nitride and graphitized carbon black and characterized the systems as being best represented by a two-dimensional film model. Cochrane, *et al*. (23) concluded from entropy calculations that the adsorption of xenon on carbon black was of the two-dimensional mobile film type. Ehrlich and Hudda (24) directly observed both patchwise and mobile adsorption for xenon on the tungsten tip of a field emission microscope at 79°K. Calculations of Hill (25) show that the transition from localized to mobile adsorption in the first layer takes place at rather low temperatures for potential barriers of around 1000 cal./mole or less. Localized physical adsorption should be a very rare phenomenon at the temperatures usually employed in adsorption experiments.

ROSS AND OLIVIER MODEL FOR MONOLAYER ADSORPTION

Ross and Olivier (9) have postulated that the solid surface is composed of very small "homotattic" patches (a patch having its own uniform adsorptive potential) that adsorb independently of each other. The Gaussian probability function was chosen to represent the continuous distribution of adsorption potentials over the surface where f_i is the frequency of a particular surface patch according to

$$f_i = \frac{d\delta_i}{dU_o} = \phi(U_o). \tag{8}$$

The term $d\delta_i$ represents the fraction of the surface having an adsorptive potential between U_{oi} and $(U_{oi} + dU_o)$. It is a necessary condition that the summation of $d\delta_i$ over all permitted values of U_o be equal to unity.

$$\int_e^g \phi(U_o)dU_o = 1 \tag{9}$$

The terms *e* and *g* represent truncation values of the Gaussian curve where $f_i = 0.001$ in Equation (8).

The Gaussian probability function was used in the form

$$f_i = \phi(U_o) = \left(\frac{1}{n}\right)\left(\exp^{(-\gamma(U_{oi}-U_o')^2)}\right) \tag{10}$$

where U_o' represents the mean adsorptive potential, γ, the heterogeneity factor, and *n*, the normalizing factor according to

$$n = \int_o^5 \exp^{(-\gamma(U_o-U_o')^2)} \, dU_o \tag{11}$$

Instead of allowing U_{oi} to vary from zero to infinity, Ross and Olivier (9) confined the range of the distribution from 0.0 to 5.0 kcal./mole. For generation of model values U_o' was chosen as 2.5 kcal./mole. Generated distributions for various γ values are shown in Fig. 1. It can be seen that low γ values are characteristic of a heterogeneous surface while high γ values (over 100) indicate homogeniety.

For each distribution curve, the total surface was divided into 50 finite patches, each defined as $\Delta\delta_i$, where

$$\Delta\delta_i = \int_{U_{oi}}^{U_{oi}+\Delta U_o} d\delta_i = \int_{U_{oi}}^{U_{oi}+\Delta U_o} f_i \, dU_o \ . \tag{12}$$

To generate a model isotherm, every patch was treated as an individual homotattic surface of energy U_{oi} for which the amount adsorbed at a given pressure *p* could be calculated from the Hill-deBoer equation (see below) using

$$K_i = A^o \exp^{(-U_{oi}/RT)} \tag{13}$$

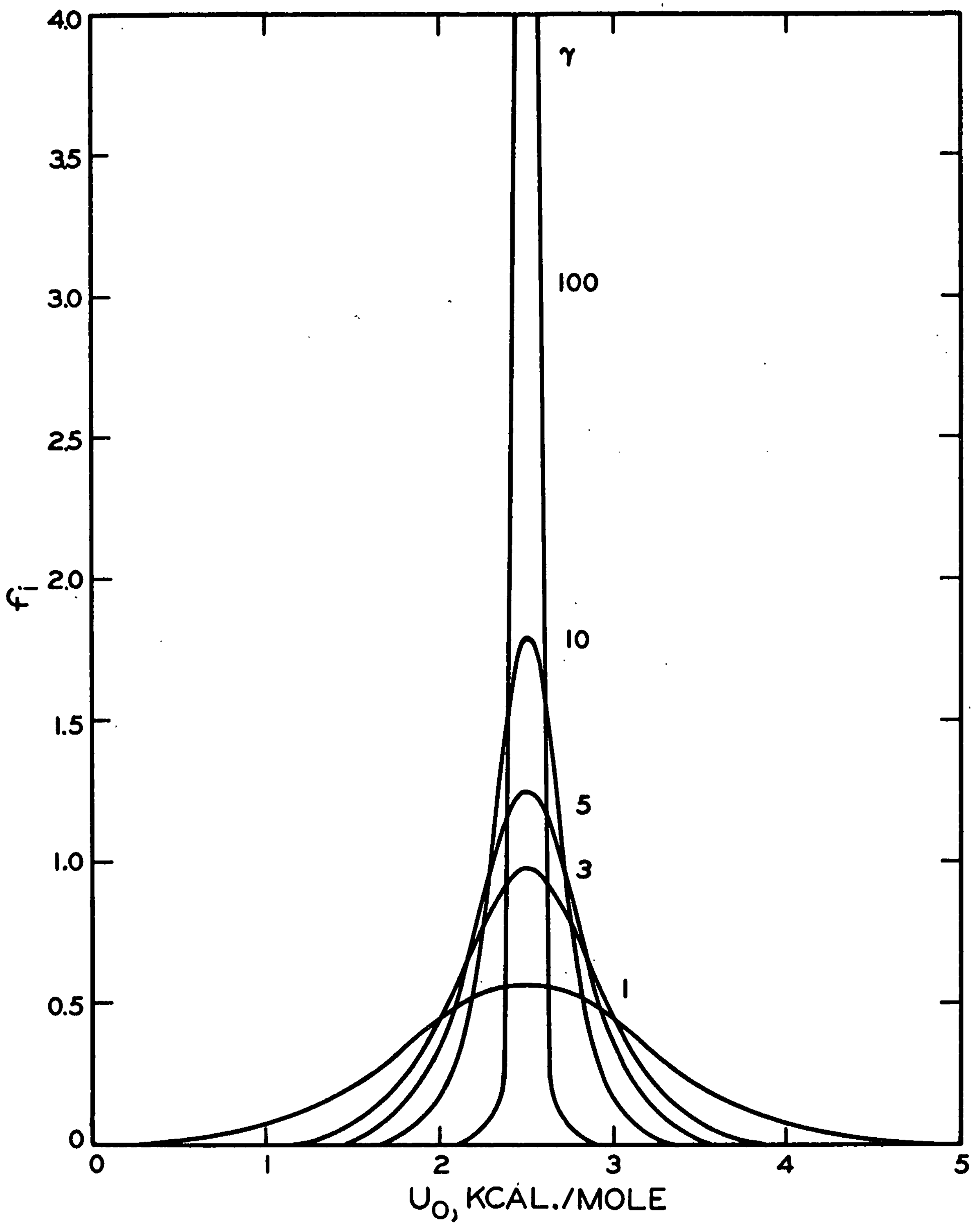

Figure 1. Gaussian Distributions of Adsorptive Potential Energies for Various Values of γ in Equation (10) [After Ross and Olivier (9)]

It is possible to calculate the value of $\underline{A}^{o}$ from the model with free energy and entropy considerations for simple cases such as atomic gases. However, for model isotherm generation, the authors arbitrarily chose a value of $\underline{A}^{o}$ so as to make $\underline{K}_i = 1$ when $\underline{U}_{oi} = \underline{U}'_o = 2.5$ kcal./mole and $\underline{T} = 77.5^\circ$ in Equation (13).

The Hill-deBoer equation is representative of mobile adsorption with lateral interaction on a homogeneous surface and may be presented in the form

$$p = K_i[\theta_i/(1-\theta_i)]\exp^{\theta_i/(1-\theta_i)}\exp^{-2\alpha\theta_i/RT\beta} \tag{14}$$

where

$\underline{p}$ = equilibrium pressure

$\underline{K}_i$ = constant related to $\underline{U}_{oi}$ of each patch

θ_i = degree of monolayer completion for a given patch

$\underline{R}$ = gas constant

$\underline{T}$ = absolute temperature

and

$$\alpha = \pi C/4d^4 \tag{15}$$

$$\beta = \pi d^2/2 \tag{16}$$

where $\underline{C}$ is proportional to the square of the polarizability of the molecule, and $\underline{d}$ is the effective molecular diameter for spherical isotropic molecules. Ross and Olivier (9) used Equations (13) and (14) to calculate the degree of monolayer completion of each homotattic patch θ_i for all values of $\underline{U}_{oi}$ from a particular distribution curve. The overall monolayer coverage, Θ, was determined using

$$\Theta = \Sigma\Delta\delta_i\theta_i. \tag{17}$$

This procedure was repeated for several assumed pressure values [$\underline{p}$ in Equation (14)] so that model isotherms of the form Θ vs. $\underline{p}$ could be obtained.

Ross and Olivier (9) have supplied over 100 pages of tabulated model isotherms with their monograph. Each table is in the form of p/K' vs. Θ for a wide range of γ values. Tables were presented for levels of $2\alpha/RT\beta$ from 0.10 to 10.00 in intervals of one-tenth.

To interpret experimentally obtained isotherms in terms of the Ross and Olivier (9) theory, it is necessary to first compare the experimental isotherm with a whole series of model isotherms until the best fit is obtained. This is generally done by plotting standard isotherms for several γ values at one $2\alpha/RT\beta$ level on a large sheet of paper in the form $\ln\Theta$ vs. p/K'. The experimental isotherm is placed on a sheet of tracing paper in the form $\ln v$ vs. $\ln p$ where v is the volume adsorbed. The scales of the two plots must be identical. The experimental isotherm is compared with the model isotherms until a match is obtained. When a match has been obtained, the displacement of the zero points on each vertical axis represents $\ln V_\beta$, the natural log of the monolayer capacity. The difference between zero points on the horizontal axis gives $\ln K'$ which is related to the mean adsorptive potential, U_o'. The γ value is characteristic of the particular model isotherm that was used for the match. An illustration of the matching procedure is shown in Fig. 2.

Once a match has been obtained, it is then possible to compare the theoretical with the experimental isotherm in the form v, the volume adsorbed, vs. p, the equilibrium pressure. The obtained parameters characterize the surface as to monolayer capacity, width of adsorptive potential range, and mean adsorptive potential.

Certain thermodynamic considerations, necessary to determine the applicability of the theory to a given adsorption system, will be discussed in a later section.

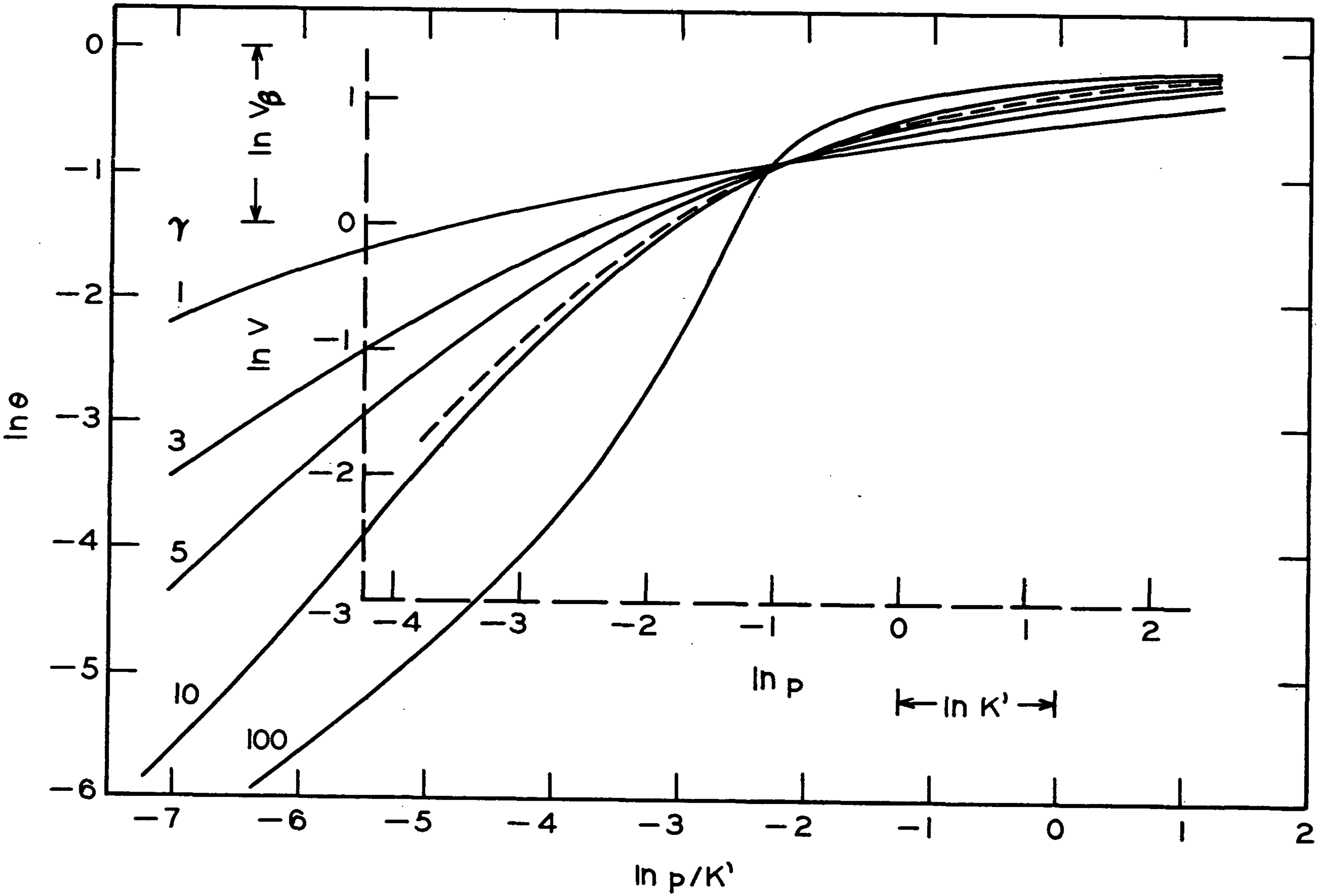

Figure 2. Model Isotherms (Solid Lines) and a Superimposed Experimental Isotherm (Dashed Line) in its Proper Interpolated Position [After Ross and Olivier (9)]

GENERAL EXPERIMENTAL PROCEDURES

SAMPLE PREPARATION

COTTON

Unpurified cotton was initially selected as a source of cellulose. It does not contain hemicelluloses, lignin, or uronic acids, which might be expected to significantly alter the energy site distribution of pure cellulose. Certain waxes and pectic substances are present, but practically all these are removed during mild purification (26). The cotton used in this study was of the same origin as that used by Sommers (26).

Purification

The raw cotton was purified using Sommers' modification of the method of Conrad (27). Essentially, the purification procedure consisted of a hand-sorting operation, followed by extraction with 95% ethanol, 1.0% boiling sodium hydroxide, and finally 0.5% acetic acid.

Solvent Exchange and Drying

A solvent-exchange and drying apparatus was constructed with only slight variation from the design of Sommers (26). The apparatus was constructed out of pyrex glass with either ground glass or blown glass joints in any areas where solvent might contact the glass. The apparatus in its final form is shown in Fig. 3. Modification of Sommers' original design consisted of replacing ball and socket joints with ground glass joints and adding of a second 10/30 joint ahead of Stopcock 3 to permit the simultaneous solvent exchange and drying of two samples.

Sample bulbs were constructed and filled using the method outlined by Sommers (26). Solvent exchange was carried out in the sequence: water — methanol — dried methanol — _n_-pentane — dried _n_-pentane, followed by drying with phosphorus pentoxide-

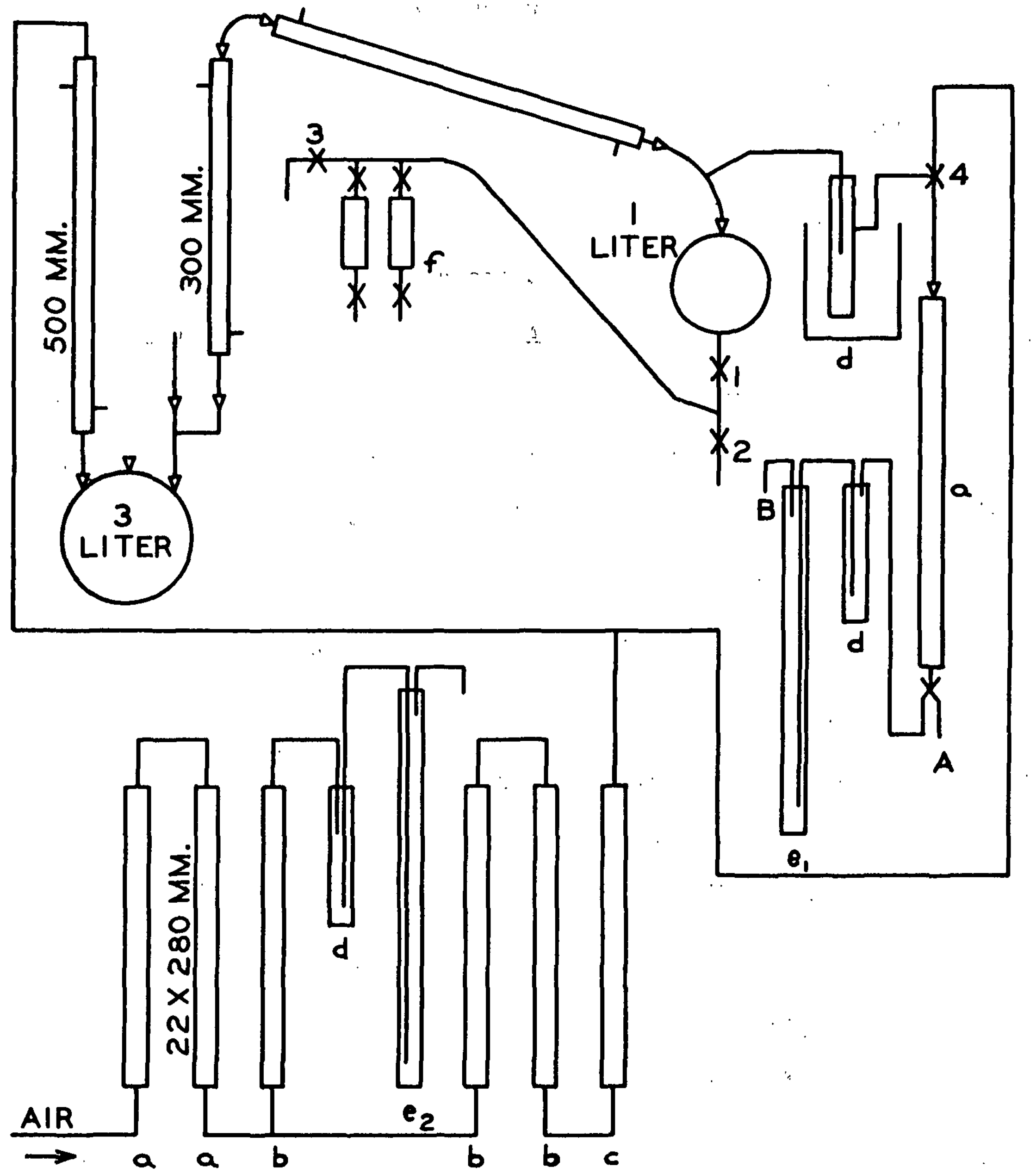

▷ GROUND GLASS JOINT
a DRIERITE
b ANHYDRONE
c PHOSPHORUS PENTOXIDE
d TRAP
e BUBBLER
f SAMPLE BULBS
X STOPCOCKS

Figure 3. Solvent-Drying and Exchange Apparatus

dried nitrogen. The dried methanol was prepared by the method of Lund and Bjerrum (28), while n-pentane was dried by refluxing over extruded sodium. Reagent-grade methanol, Phillips 66 research grade n-pentane, and Matheson prepurified nitrogen were employed for each solvent exchange and drying operation. At no time during the solvent exchange and drying procedure was the sample allowed to come in contact with atmospheric moisture.

The number of exchanges employed and the contact times of solvent to sample varied somewhat for different samples. A complete description of the solvent-exchange and drying procedure for each sample is given in the Appendix. The number of exchanges and the solvent-sample contact times were decided upon through consideration of the findings of Merchant (29) and Sommers (26).

Humidification and Drying

The work of Merchant (29) has shown that the exposure of a solvent exchange dried cellulose sample to atmospheric moisture with subsequent redrying resulted in a decrease in the surface area of the sample. To investigate possible changes in the character of the cellulose surface as a function of the surface area developed, it was decided to expose a WAN dried sample to different relative humidities, to redry, and to obtain adsorption isotherms. Initial humidification (at 50% R.H.) and redrying should also remove any residual solvent that remained on the sample as a result of the solvent exchange procedure.

Samples B1 and B3 were solvent exchanged and dried according to the schedules listed in Tables XII and XIV. After the necessary adsorption data were collected for solvent exchange-dried Sample B3, it was placed in a 50% R.H. room with the stopcock open. The sample was subjected to cycling evacuations with subsequent exposures to 50% R.H. air over a three-day period. Although true equilibrium was probably not obtained, it was felt that this exposure to water vapor should have been sufficient to reduce the surface area significantly. For adsorption run purposes, this sample was then labeled B3-H50.

Following the collection of adsorption data for B3-H50 (Table XIII), the sample was subjected to evacuation-exposure cycles with 86.5% R.H. air. The 86.5% R.H. air was maintained using a saturated potassium chromate solution. The cycling was accomplished using a three-way stopcock that was connected to a vacuum line, to the sample, and to a two-liter flask containing the saturated potassium chromate solution. The cycling was carried out by simple adjustment of the stopcock. The sample was subjected to periodic cycling over a two-day period. The purpose of the cycling was not to equilibrate the sample with 86.5% R.H. air which would have required several weeks but merely to reduce the sample surface area. This sample was then designated as B3-H86 (Table XVI).

WATER-DRIED COTTON

A sample of purified cotton was dried directly from water in an adsorption bulb by the passage of phosphorus pentoxide-dried nitrogen through the bulb. The sample was labeled B4.

OXIDIZED COTTON

To investigate the effects of changing the chemical composition of the cellulose surface on the determined energy site distribution, an oxidized cellulose was prepared.

The procedure of Nevell (30) was followed for the periodate oxidation of about 10 g. of purified cotton cellulose. The reaction was carried out in a 1 qt. Mason jar which had been covered with tinfoil to exclude light. Initial and final periodate concentrations were determined volumetrically by addition of potassium iodide to aliquots of reaction solution and titration with sodium arsenite.

The oxidized cotton, Sample BO-1, was then solvent exchanged and dried as outlined in Table XVIII.

RAYON

A supply of both viscose rayon and high tenacity viscose rayon was obtained from the FMC Corporation. Batches of each type were washed thoroughly in a Buchner funnel with several liters of hot water. The rayon samples were loaded into the sample bulbs in a wet condition and then dried by the passage of phosphorus pentoxide-dried nitrogen through the bulbs at a rate of 50 cc. per minute for at least 17 hours. Samples prepared in this fashion were designated as "water dried" as opposed to "solvent exchange dried." The high tenacity rayon and the normal rayon were labeled as B5-RAY and B6-RAY, respectively. Both rayons had a denier value of 1.5.

HYDROXYETHYLATED COTTON COMBERS

A supply of hydroxyethylated cotton combers were obtained from Didwania (31) who studied the effects of hydroxyethylation on bonding properties. Didwania found an increase in bonding strength values as a result of hydroxyethylation. It was thought that the energy site distribution of such chemically modified fibers would be of interest. The degree of hydroxyethylation of the sample selected was 0.23. Following water drying, the sample was labeled B-HYD1.

INCENSE CEDAR CHLORITE HOLOCELLULOSE

Incense cedar chlorite holocellulose was obtained from Thompson (32). Of interest were possible changes in adsorption parameters as a result of the presence of hemicelluloses. The sample was water dried and designated B-HOLO1.

TITANIUM DIOXIDE

Titanium dioxide, obtained by Williams (33) from the Glidden Company, was chosen for the adsorption study. This particular supply which has been characterized by geometric and sedimentation measurements by Williams and Webb (33) was RG grade anatase. The sample, designated B-$T_1O_2$1, was loaded into the adsorption bulb in the dry state.

CHOICE OF ADSORBATE

To simplify the interpretation of adsorption data using the theory of Ross and Olivier (9), it is necessary that the adsorbate molecule be spherical so that the rotational entropy change due to restricted rotation upon adsorption will be zero. When this is not the case, an estimate of the surface electric field strength is necessary to calculate the rotational entropy change. Although it was pointed out previously that the adsorption of nitrogen on cellulose may be characterized as heterogeneous with lateral interaction, nitrogen is not a suitable adsorbate for Ross and Olivier (9) interpretation since estimates of the surface electric field strength of cellulose are not available.

Argon was chosen as the gas to be employed in the initial adsorption studies. It was thought that the present adsorption apparatus would lend itself to argon adsorption since the vapor pressure of argon is sufficiently high at both liquid nitrogen and liquid oxygen temperatures.

Matheson prepurified argon was obtained for the adsorption studies.

MEASUREMENT OF ADSORPTION ISOTHERMS

APPARATUS

The adsorption apparatus used for this study was essentially that of Haselton (4) with minor modifications made by Merchant (29). The apparatus was originally designed for B.E.T. measurements and includes a McLeod gauge, two mercury manometers, and a gas buret. Since a complete description of both the design and operation of this apparatus has been presented by previous workers (4, 29), this will not be considered in detail here. A diagram of the apparatus is shown in Fig. 4.

OPERATION OF ADSORPTION APPARATUS

Outgassing

Cellulosic samples were outgassed for at least twelve hours and were heated to 70°C. during the outgassing period. Adsorption runs were never started unless the pressure in the system was less than 2.0×10^{-6} mm. Hg. The titanium dioxide sample was outgassed at 150°C. for at least 12 hours.

Deadspace Determinations

Duplicate deadspace determinations were made with Matheson prepurified helium on each sample at the particular bath temperature to be employed for argon adsorption on that sample. Results were expressed in ml./mm. and are presented in the Appendix.

Collection of Adsorption Data

The method of operation of the adsorption apparatus varied for different samples depending on the surface area available. For samples having very low surface areas, only the two smallest bulbs of the gas buret were employed for duplicate dosing and equilibrium measurements. For large surface area samples, more and larger bulbs were used for dosing the larger volumes required. At equilibrium, the mercury level was always lowered to the bottom of the gas buret, B. For measurement of equilibrium pressures, the gas buret was isolated from the sample by means of stopcock S_2 and the mercury raised to the upper bulbs for duplicate pressure measurements. The advantages of this method were that large volumes could be added, low equilibrium pressures could be readily attained, and

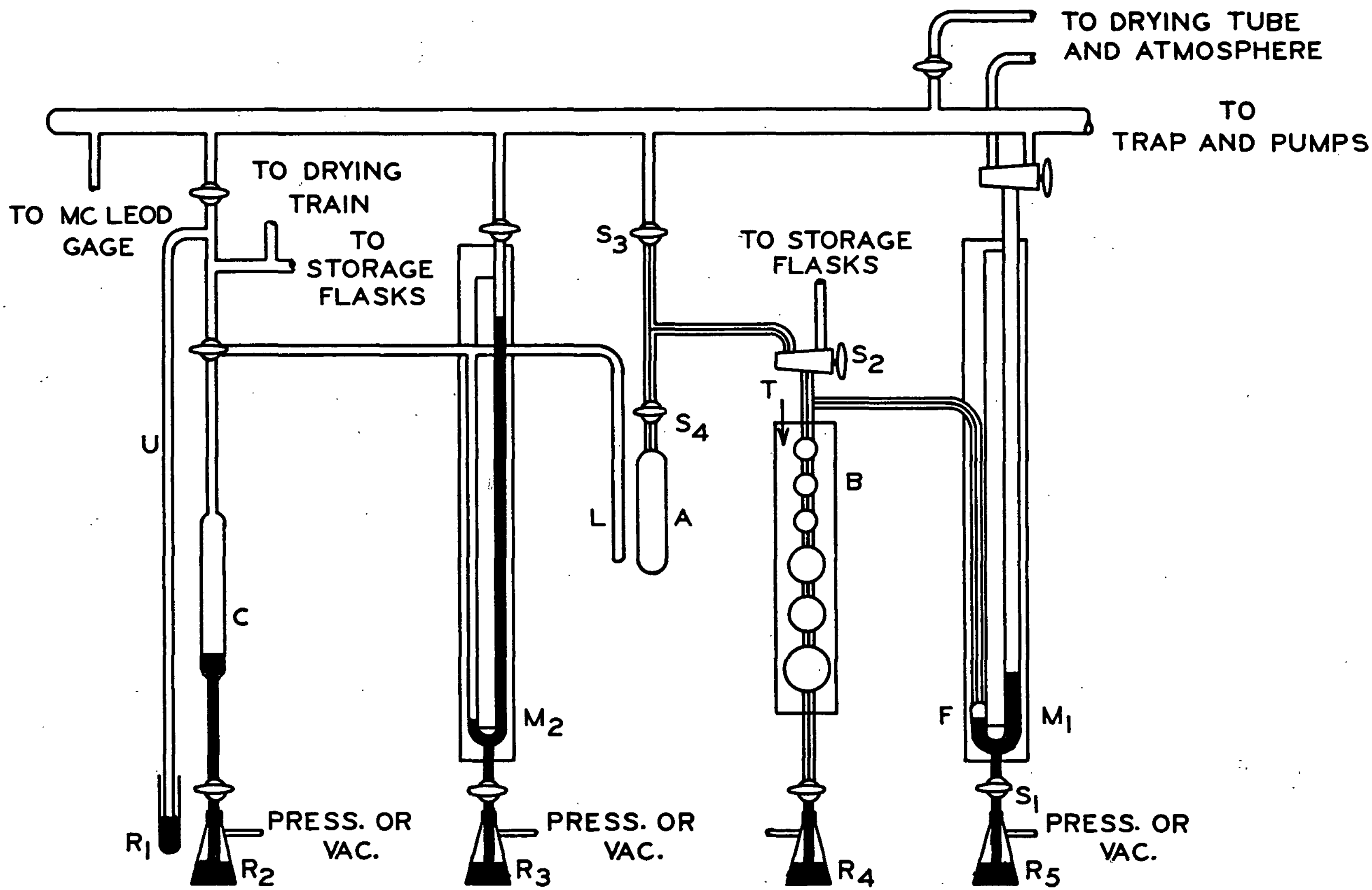

Figure 4. Apparatus for Determination of Adsorption Isotherms. A - Sample Bulb; B - Gas Buret in Water Jacket; C - Compression Bulb; F - Fiducial mark; L - Condensation Leg for Adsorbate; M_1,M_2 - Mercury Manometers; R_1,R_2,R_3,R_4,R_5 - Mercury Reservoirs; S_1,S_2,S_3,S_4 - Stopcocks; T - Thermometer; U - Barometric Dropleg

the compression of the gas in the buret following equilibrium permitted a large magnification of the mercury manometer reading. This procedure may be called a combination of the constant mass and constant volume methods since duplicate pressure measurements were always attainable, but yet the mass of the gas in the system had to be increased for each isotherm point.

Either liquid nitrogen or liquid oxygen was used to control the sample bulb temperature during adsorption runs. The saturation pressure of argon was determined manometrically for each adsorption run at liquid nitrogen temperature. A nitrogen gas thermometer was used when accurate measurement of the bath temperature was required.

Generally, isotherm data were collected for an equilibrium pressure range of from 1.0 to at least 70 mm. Hg. On some occasions a much broader range of pressures was studied.

Determination of Sample Weight

Following an adsorption run, the sample bulb was removed from the apparatus and cracked open with a hot nichrome wire. The sample was removed, placed in a weighing bottle, and heated at 105°C. for 2 hours. Following the heating period, the sample was removed from the oven, allowed to cool in a desiccator, and then weighed. Results of the weighings are listed in the Appendix.

SORPTOMETER

A few trial adsorption runs were made using the sorptometer which has been described by Didwania (31). A controlled stream of 15% nitrogen and 85% helium was passed through the sample which was in a liquid nitrogen temperature bath. The exit stream concentration was continuously monitored by a thermal conductivity cell. Whatman No. 1 filter paper, which had been characterized by means of B.E.T.

analysis of volumetric adsorption measurements, was used as the area standard for the sorptometer runs.

DETERMINATION OF GEOMETRIC SURFACE AREAS

RAYON FIBERS

Estimates of the geometric surface areas of both the normal viscose rayon sample and the high tenacity viscose rayon sample were obtained. The procedure was identical for both samples. Fibers were mounted in methyl methacrylate with their axes nearly parallel. A perpendicular cross section was obtained with a microsectioning apparatus and mounted on a glass slide. Images of the fiber cross sections, magnified 750X, were focused on a frosted glass plate. A sufficient number of fiber perimeters were then copied onto tracing paper. These tracings were then magnified and focused onto large sheets of paper by means of an overhead projector. Fiber perimeters were determined using a map tool while fiber cross sections were obtained with a planimeter. Both perimeters and cross sections were measured in duplicate and then averaged for each fiber. Surface areas were calculated using the average fiber perimeter and an estimate of the sample density. Details of the calculation are shown in the Appendix in Tables XXI and XXII. Regular and stereo electron micrographs were prepared from surface replicas of both the normal and high tenacity rayon. A number of magnifications were employed. A number of high tenacity rayon fibers were mounted in epon 812, celloidin, and butyl methacrylate. Visual measurements by the optical microscope indicated that the average fiber diameter was independent of the mounting medium.

TITANIUM DIOXIDE

An estimate of the geometric surface area of the titanium dioxide sample was obtained from Webb (33), who measured over 1200 particle diameters using electron micrographs.

EXPERIMENTAL RESULTS AND DISCUSSION

CURVE MATCHING CONVENTION

Ross and Olivier (9) have made it quite clear that application of their theory becomes increasingly difficult for extremely heterogeneous substrates. For very heterogeneous adsorbents a plot of ln (volume adsorbed) vs. ln (equilibrium pressure) may be nearly a straight line. The problem of matching an experimental to the theoretical ln-ln plot will now, of course, be quite difficult since many combinations of the parameters exist that will give good agreement with the observations. When this difficulty was encountered in curve matching, the following convention was employed:

> The experimental ln-ln plot was matched with the theoretical ln-ln plot with the position of the experimental plot as far to the right as possible. Use of this convention resulted in minimum values of V_β and maximum values of U_o'. Since multilayer adsorption was observed at low monolayer completions (which will be discussed in detail later) resulting in an inflection point in the ln-ln plots, this convention allowed for making use of the greatest part of the monolayer part of the ln-ln curve possible. The choice of this convention was based on previous matching experiences where adsorbents possessing identical U_o' values, but different γ values were involved.

CONFIRMATION OF ROSS AND OLIVIER CASE I ANALYSIS

THE ANALYSIS OF K'

The parameter K' is defined by Equation (18):

$$K' = A^o \exp^{(-U_o'/RT)} \qquad (18)$$

Where, for the mobile adsorption model

$$\ln A^{o} = -\left[\frac{\Delta S_{s}^{tr}+\Delta S^{rot}}{R}\right] + \frac{aF^{vib} - aE_{o}^{vib}}{RT} + \frac{\Delta E^{kin}}{RT} - \ln\frac{\theta_{s}}{1-\theta_{s}} + \ln 760 \qquad (19)$$

In Equation (19),

$-\Delta S_{s}^{tr}$ = represents the integral translational entropy change per mole of a gas in its standard state (760 mm., temperature = T) to a mobile adsorbed film in its standard state (θ_s,T)

ΔS^{rot} = change in rotational entropy on adsorption

aF^{vib} = additional Gibbs free energy of the adsorbed phase due to molecular vibrations with respect to the surface

aE_{o}^{vib} = average vibrational energy of the adsorbed molecule

ΔE^{kin} = the difference between the total kinetic energy per mole of a molecule in the gas phase and the kinetic energy of translation and rotation per mole of a molecule in the adsorbed phase

θ_s = standard state of the surface phase, taken so that the average intermolecular separation would be the same in both the gas and adsorbed phases at 0°C.

The analysis of K' can be quite difficult or relatively simple, depending on the amount of adsorption data available at different temperatures and on the complexity of the adsorbate molecule. The choice of a spherical monatomic gas, such as argon, for adsorption at low temperatures, has been characterized by Ross and Olivier (9) as Case I analysis. This case allowed for the simplest interpretation of adsorption data.

For argon adsorption at 77.5°K., $\Delta S^{rot} = 0$.

$$-\Delta S_{s}^{tr} = \frac{R}{2}\ln M + \frac{R}{2}\ln T + 2.30 \qquad (20)$$

where M refers to the molecular weight of argon.

$$\Delta E_{kin} = -\frac{1}{2}RT \qquad (21)$$

$$aF^{vib} - aE_o^{vib} = RT \ln (1 - \exp^{(-h\nu/kT)}) \simeq 0 \qquad (22)$$

with

$\underline{h}$ = Planck's constant

ν = vibrational frequency with respect to the surface of the adsorbed molecule

$\underline{k}$ = Boltzmann constant

Under these conditions, Equation (19) reduces to

$$\ln A^o = -\frac{\Delta S_s^{tr}}{R} - 0.5 - \ln \frac{\theta_s}{1-\theta_s} + \ln 760. \qquad (23)$$

By making use of the above assumptions, $\underline{A}^o$ may be calculated for argon as a function of temperature. The simplifying assumptions are assumed to be correct if a plot of the logarithmic form of Equation (18)

$$\ln K' - \ln A^o = - U_o'/RT \qquad (24)$$

results in a straight line through the origin when plotted in the form ($\ln \underline{K}'$ - $\ln \underline{A}^o$) vs. $1/\underline{T}$.

Case 1 analysis was carried out for the adsorption of argon on Sample B1 (WAN dried cotton cellulose) at 77.5°K and at 90.1°K. Experimental values of $\underline{V}_\beta$, γ, and $\underline{K}'$ were obtained at each temperature and are presented in Table I.

The fit of the theoretical to the experimental isotherms for argon adsorption on Sample B1 at 77.5°K and 90.1°K is shown in Fig. 5 and 6, while the corresponding energy site distributions are presented in Fig. 7 and 8.

It can be seen that very good theoretical to experimental isotherm fits were obtained at both temperatures. Also of interest is the close agreement obtained for both the $\underline{U}_o'$ and the γ values. The applicability of Case 1 analysis is confirmed by

Fig. 9, where the plot of $(\ln \underline{K}' - \ln \underline{A}^{o})$ vs. $1/\underline{T}$ fits a straight line passing through the origin.

TABLE I

ROSS AND OLIVIER PARAMETERS FOR ARGON ADSORPTION
ON SAMPLE B1 AT 77.5°K AND 90.1°K

Parameter	Temperature 77.5°K	90.1°K
$\gamma_{77.5}$	2.0	1.85
$\underline{K}'$	882.0	3262.0
$\underline{V}_{\beta}$	36.4	30.2
$\underline{U}'_{o}$	1.17	1.17

The cellulose surface exhibited both a very broad range of adsorptive potentials and a very low mean adsorptive potential.

The γ value of 1.85 at 90.1°K represents the temperature corrected value. Actually a value of $\gamma = 2.50$ was obtained when matching theoretical with experimental isotherms at a $2\alpha/\underline{RT}\beta$ level of 5.60 (90.1°K, ideal values of α and β). Since the theoretical isotherms of Ross and Olivier were tabulated for 77.5°K, it was necessary to multiply the γ value obtained by $(77.5/90.1)^2$ to obtain the corrected value.

Also, since Ross and Olivier did not supply a computed theoretical isotherm at $\gamma = 2.5$, $2\alpha/\underline{RT}\beta = 5.60$, it was necessary to generate one using an IBM 1620 II Computer (Fig. 10).

A decrease in the monolayer capacity, $\underline{V}_{\beta}$, was observed for the isotherm at 90.1°K. This is believed to be due to the effects of heating and aging of the sample prior to the adsorption run at 90.1°K. Immediately after the adsorption run at 77.5°K, the sample was heated to 75°C. and outgassed for 15 hours. The sample then

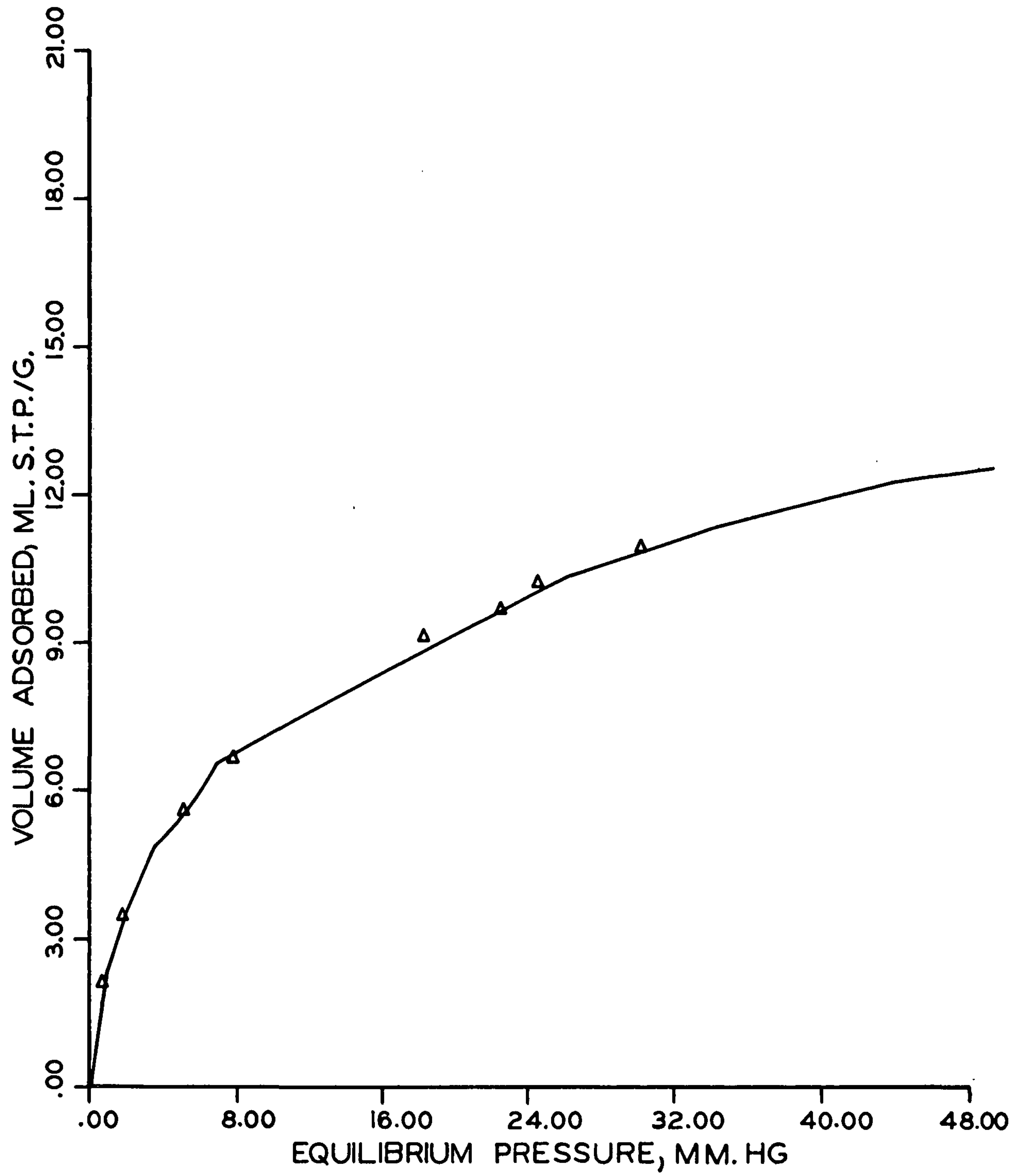

Figure 5. Theoretical and Experimental Isotherms for Argon Adsorption on Sample B1 at 77.5°K.

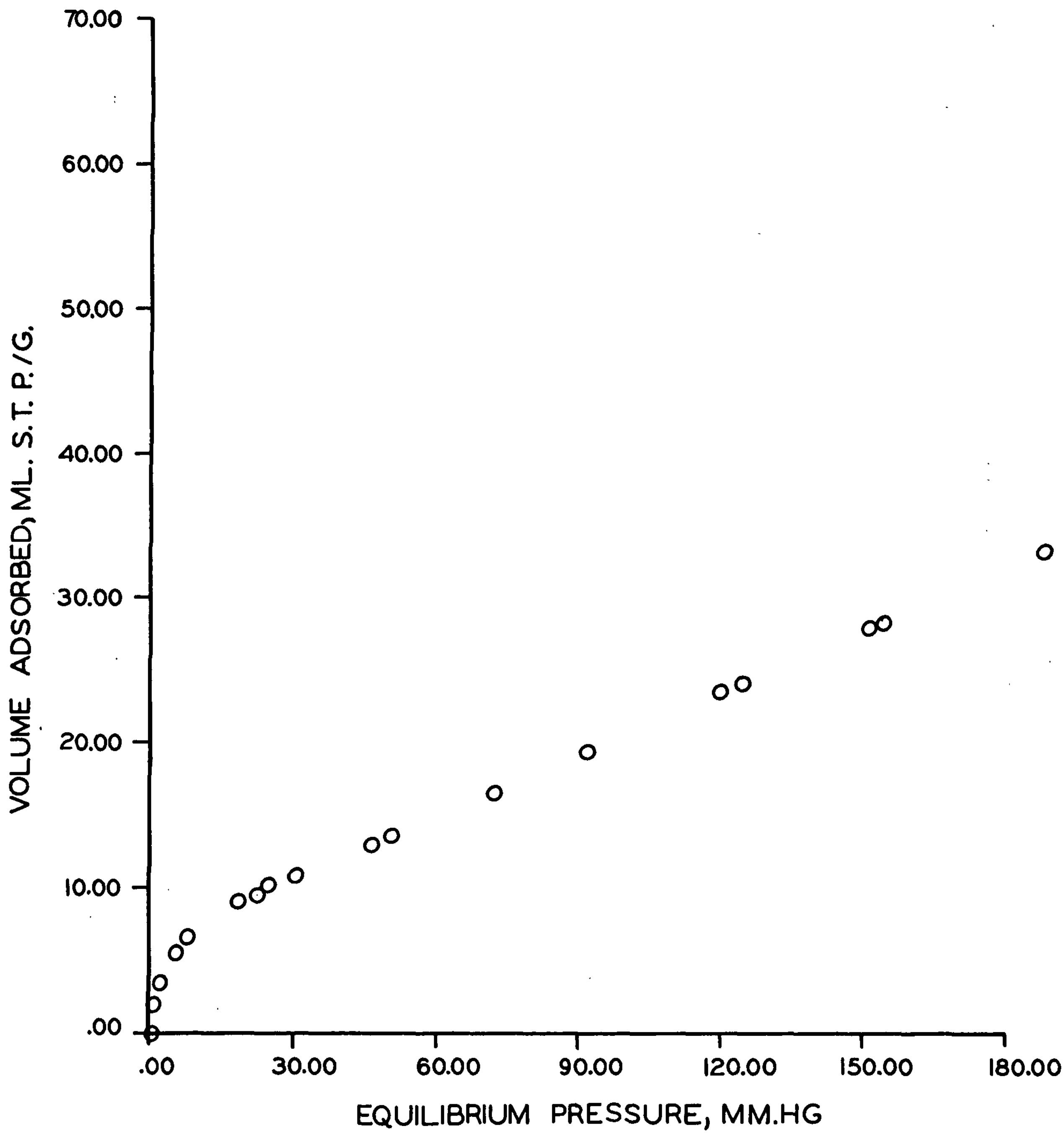

Figure 5A. Complete Experimental Isotherm for the Adsorption of Argon on Sample B1 at 77.5°K

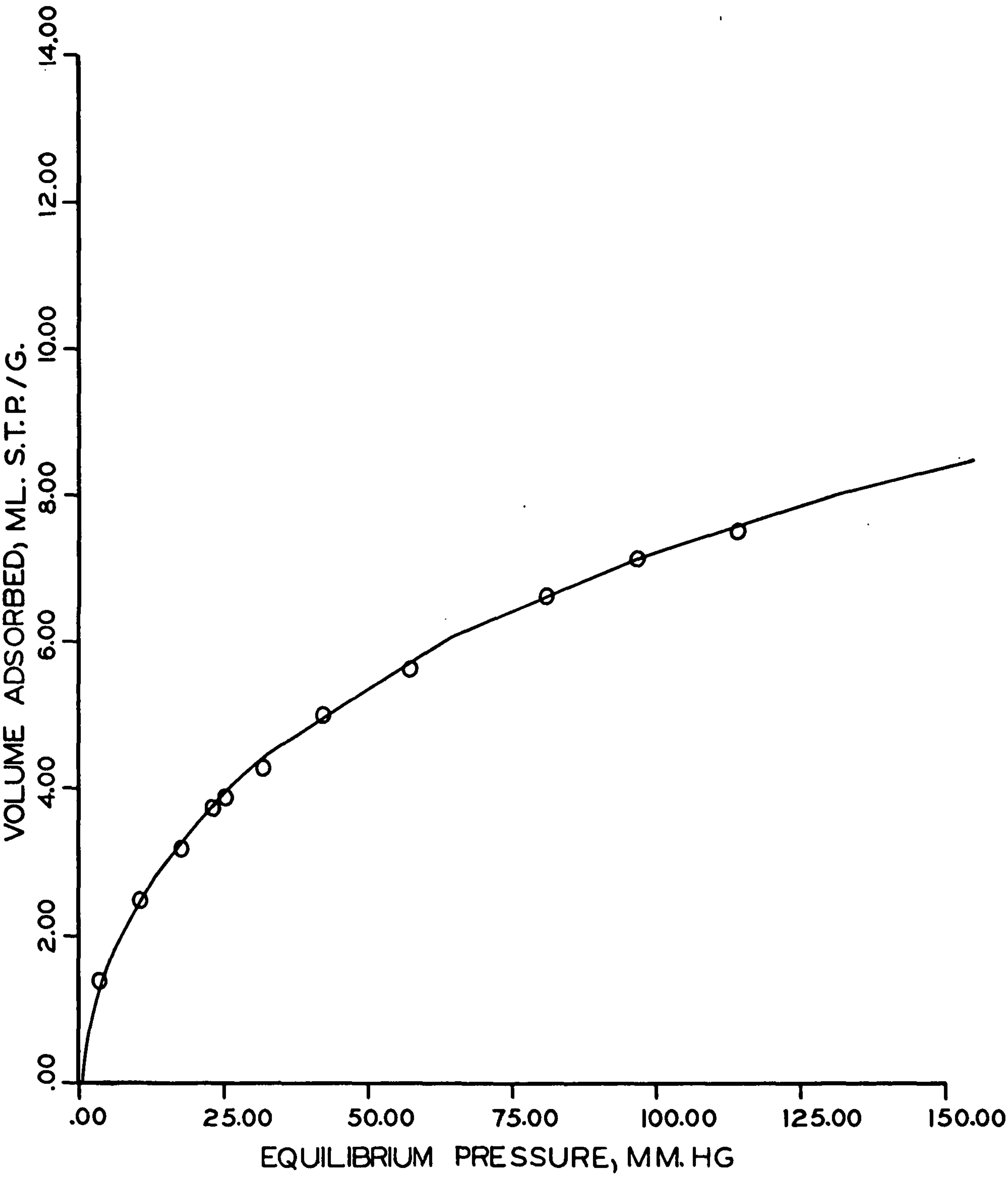

Figure 6. Theoretical and Experimental Isotherms for Argon Adsorption on Sample B1 at 90.1°K

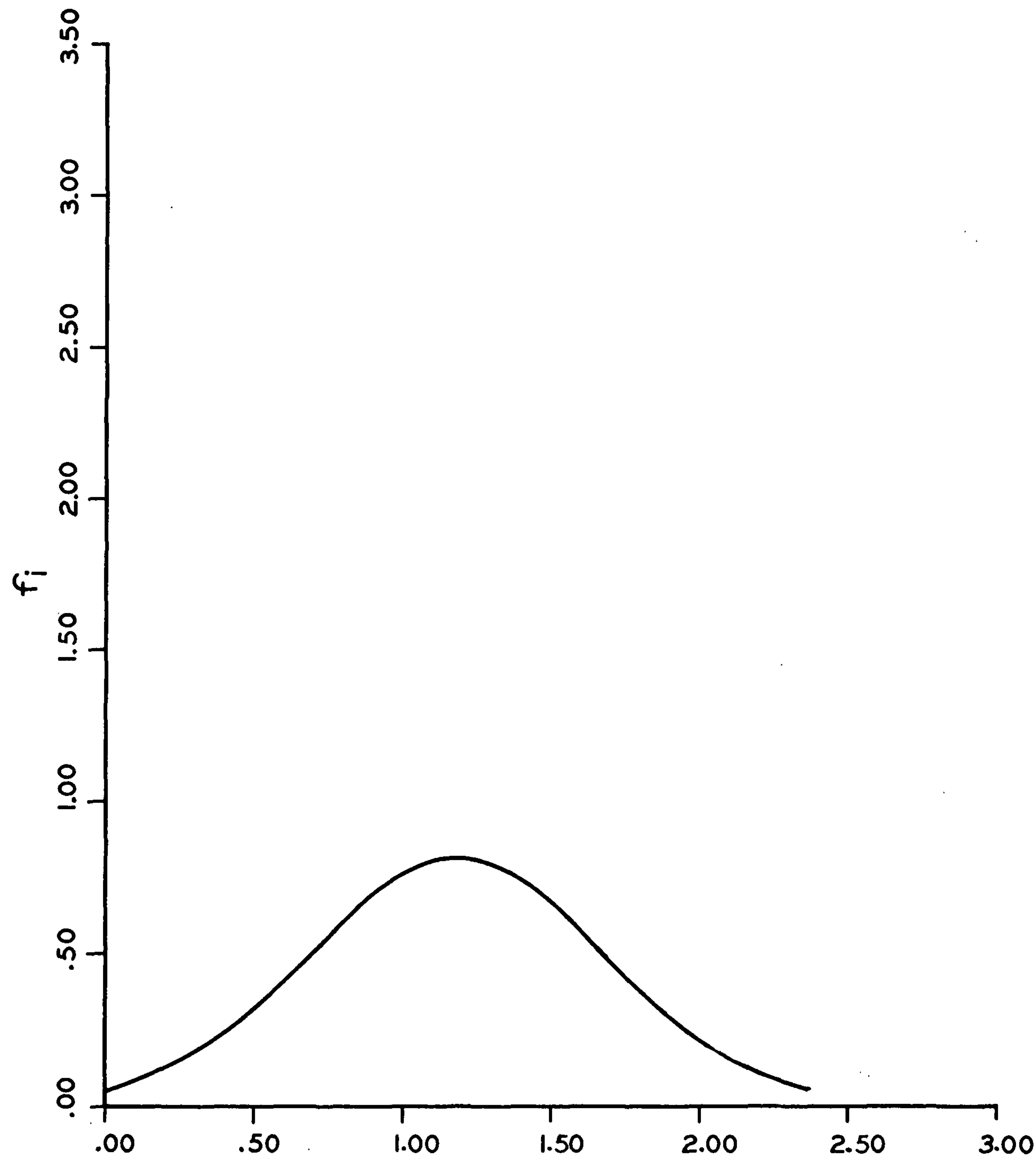

Figure 7. Energy Site Distribution Curve for Argon Adsorption on Sample B1 at 77.5°K

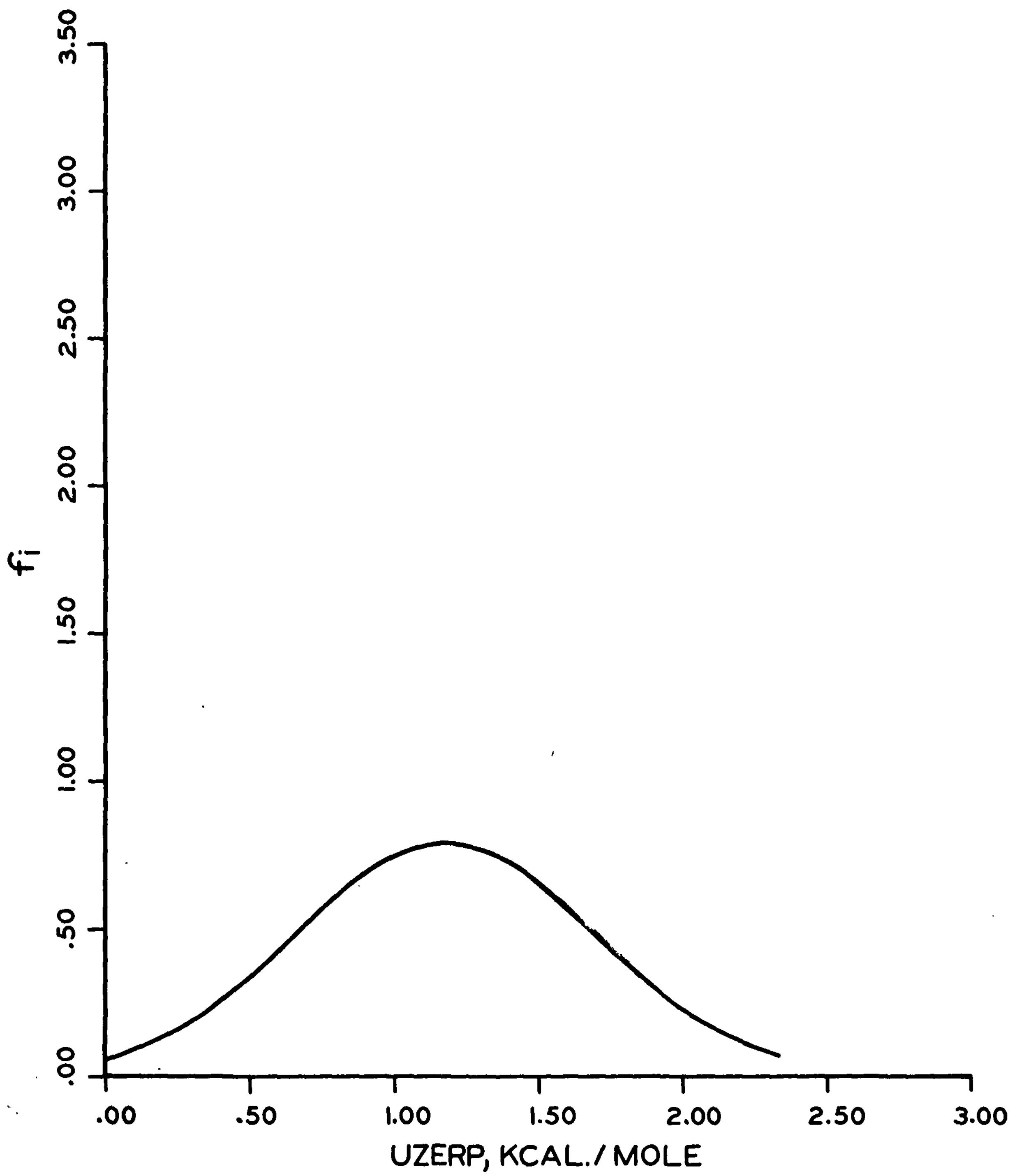

Figure 8. Energy Site Distribution Curve for Argon Adsorption on Sample B1 at 90.1°K

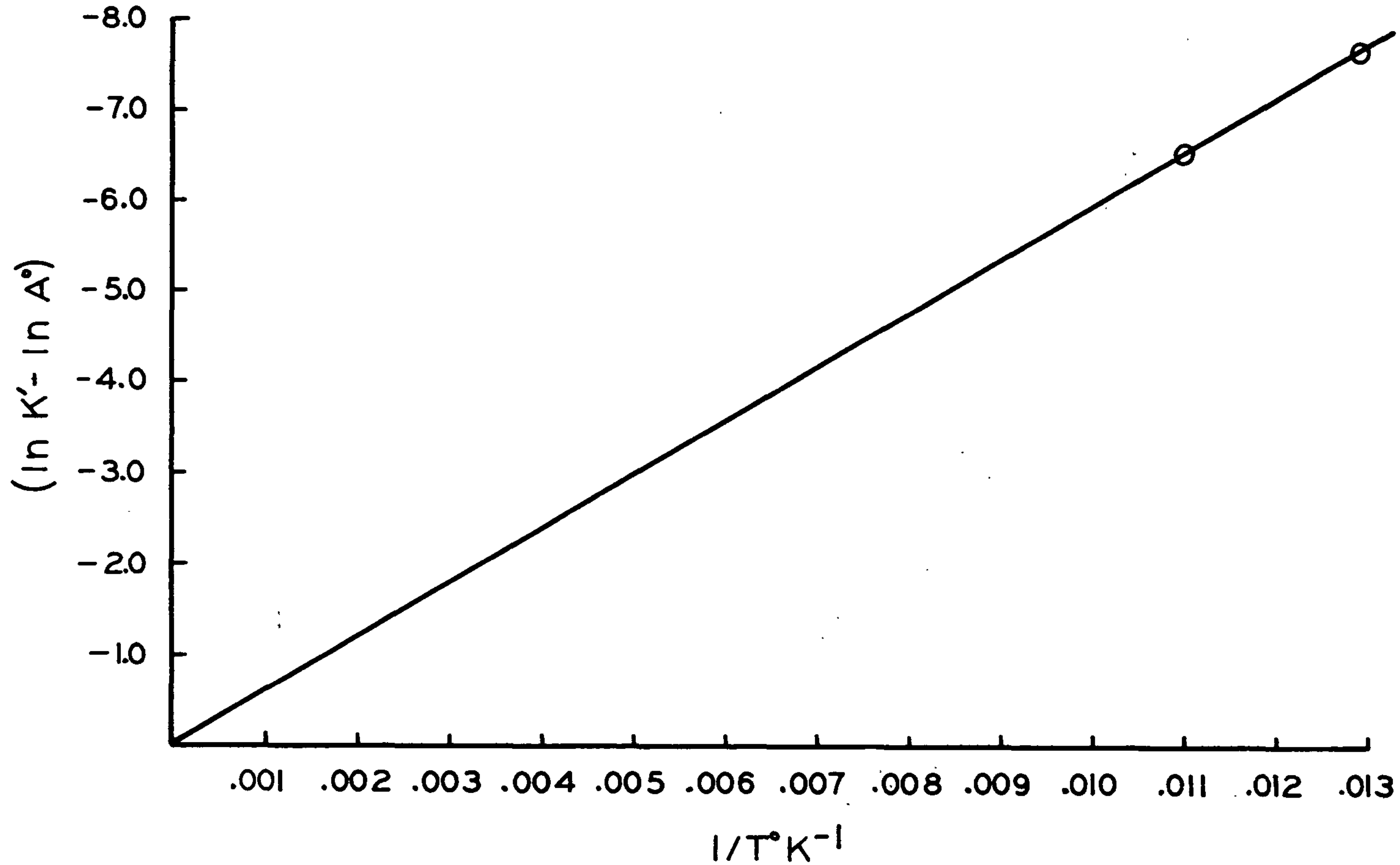

Figure 9. Plot of ($\ln \underline{K}' - \ln \underline{A}^{o}$) vs. $1/\underline{T}$ for Argon Adsorption on B1 at 77.5° and 90.1°K

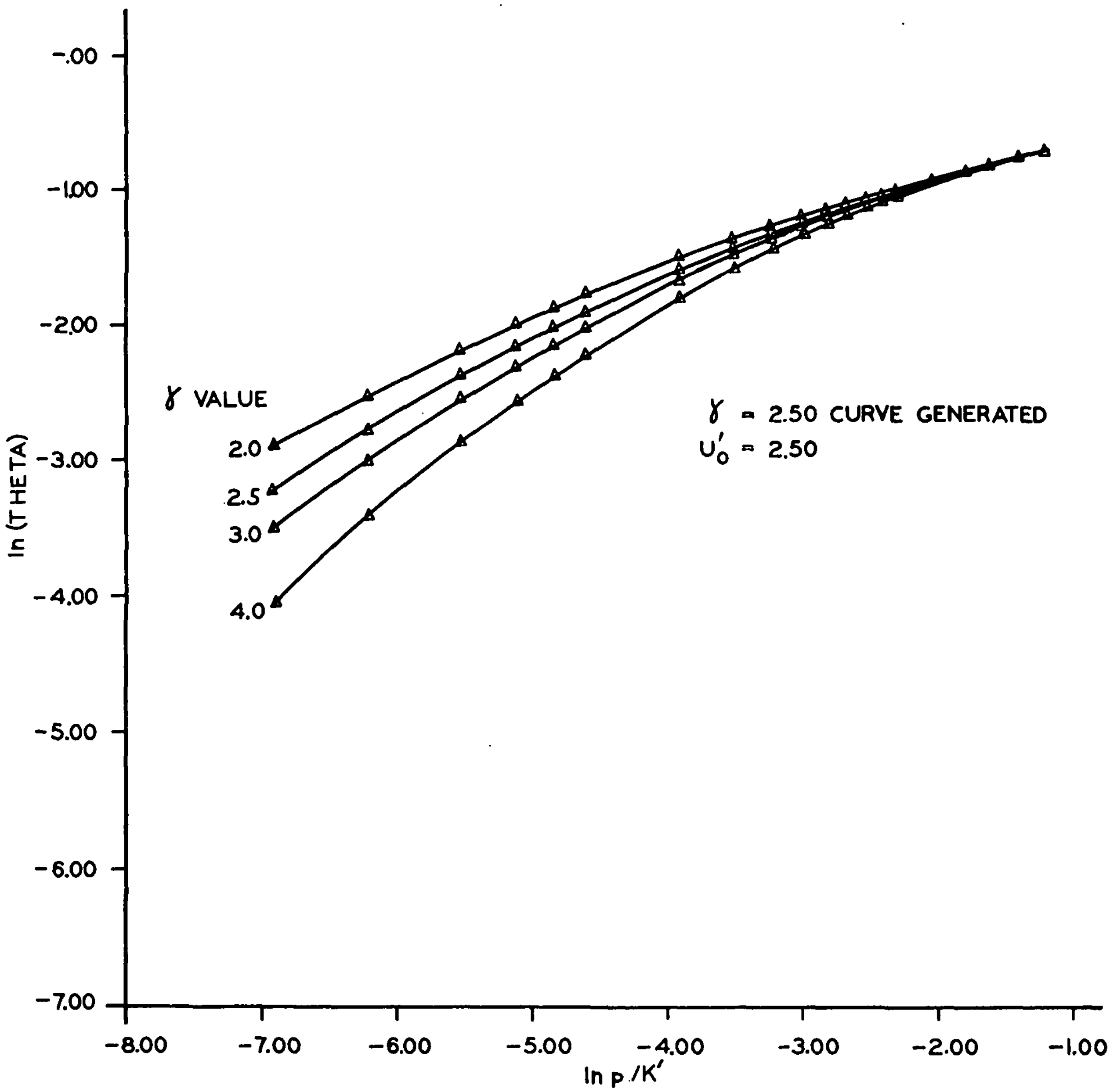

Figure 10. Generated Model Isotherm for γ = 2.50 at the 5.60 $2\alpha/RT\beta$ Level

aged eight days between the runs at 77.5°K and 90.1°K. The effects of heating and aging on the surface area of WAN dried samples was thoroughly investigated by Merchant (29). Based on his results, one could expect about a 20% decrease in surface area for Sample B1 due to the heating and aging encountered. About a 17% decrease was observed experimentally based on Ross and Olivier (9) V_β estimates.

Deitrich (34) has recently obtained adsorption isotherms for argon on WAN dried cotton cellulose at both 77.5°K and 90.1°K taking care to avoid the effects of heat and aging. Case 1 data analysis was again shown to be applicable, and identical estimates of V_β were obtained at the two temperatures employed. This also served to demonstrate the temperature invariance of the monolayer capacity estimates for a small temperature change, which is a property claimed by the model.

In Fig. 5 it should be noted that agreement between the theoretical and experimental isotherms was only possible up to a monolayer coverage of about 0.3 (corresponding to about 50 mm. Hg pressure) for the isotherm at 77.5°K. Multilayer buildup became increasingly important at equilibrium pressures greater than about 50 mm. Hg, resulting in an inflection point in the experimental isotherm. The Ross and Olivier (9) model, strictly a model of monolayer adsorption, cannot be expected to be applicable at adsorption conditions where significant multilayer buildup occurs. It is not implied that this in any way detracts from or limits the applicability of their theory for the interpretation of adsorption isotherms. It does mean, however, that for the matching of experimental to theoretical isotherms for surfaces exhibiting a low and heterogeneous adsorptive potential, only the low pressure end of the isotherm is of importance.

As pointed out by Ross and Olivier (9), the matching procedure becomes increasingly inaccurate as the heterogeneity of the surface increases (i.e., lower γ values). This is illustrated in Fig. 2, where it is seen that the model curves become more horizontal with less curvature for lower γ values. Due to this it becomes more difficult to find a unique match between theoretical and experimental isotherms, and, in some cases, several "matches" may exist. This difficulty may be partially overcome by:

1. Collecting adsorption data over a sufficiently large pressure range, and at more than one temperature.
2. Employing a higher temperature for adsorption. This has the effect of making the surface appear to be more homogeneous, thus increasing the curvature of the $\ln v$ vs. $\ln p$ plot.
3. Experience in the matching procedure.

ISOSTERIC HEATS OF ADSORPTION

Experimental isosteric heats of adsorption for the adsorption of argon on Sample B1 were calculated using the isotherm data collected at 77.5°K and 90.1°K. The Clausius-Clapeyron equation was used to calculate the experimental isosteric heats, q_{exp}^{st}, where

$$q_{exp}^{st} = R\,[T_1T_2/(T_2 - T_1)]\,[\ln (p_2/p_1)]. \tag{25}$$

In Equation (25), p_1 and p_2 refer to equilibrium pressures determined at constant monolayer coverage, Θ, at T_1 (77.5°K) and T_2 (90.1°K), respectively. Calculated experimental isosteric heats are shown in Table II.

Theoretical isosteric heats of adsorption were determined for the B1-argon system by the procedure outlined by Ross and Olivier. Only experimental values of γ and U_o' were required for the calculations.

First, U_{oi} values were determined at which f_i were approximately equal to 0.001 according to Equation (10), using the experimentally determined values of γ

and U_o'. These represent the truncation values for the Gaussian curve and are shown in Table III as *g* and *e*.

TABLE II

EXPERIMENTAL ISOSTERIC HEATS OF ADSORPTION FOR ARGON ON SAMPLE B1

Ross and Olivier Monolayer Completion, Θ	Isosteric Heat of Adsorption, q_{st}^{exp} kcal./mole
0.10	2.30
0.15	2.15
0.20	2.05
0.25	2.01
0.30	1.93
0.35	1.91
0.40	1.87
0.45	1.90
0.50	1.83

TABLE III

TRUNCATION VALUES FOR GAUSSIAN DISTRIBUTION CURVE FOR ARGON ADSORPTION ON SAMPLE B1 AT 77.5°K

U_{oi} Value	f_i Value
e = -0.64920837	0.00096054172
g = 3.0109114	0.00096063954

Limits of integration for Equation (11) were taken as -0.8 and 4.0 to include all the area under the distribution curve. ΔU_o of Equation (12) was taken to be (*e*-*g*/100), thus dividing the surface into 100 subdivisions, each subdivision considered to behave as a homotattic patch. The terms $\Delta\delta_i$, K_i, and θ_i were determined from Equations (12), (13), and (14).

The integral adsorptive potential, $\underset{\sim}{U}_o^{int}$, was evaluated from

$$U_o^{int} = \sum_i \Delta\delta_i \theta_i U_{oi}. \qquad (26)$$

The differential adsorptive potential, U_o^{diff}, defined as $dU_o^{int}/d\Theta$, was actually computed as $\Delta U_o^{int}/\Delta\Theta$. This permitted the calculation of the differential heat of adsorption, q^{diff}, using

$$q^{diff} = U_o^{diff} - \Delta E^{kin} + {}_aP^{ia} \qquad (27)$$

where

$${}_aP^{ia} = 2\alpha\Theta/\beta. \qquad (28)$$

Finally, the theoretical isosteric heats of adsorption, q^{st}, were determined from

$$q^{st} = q^{diff} + RT. \qquad (29)$$

Table IV includes listings of the computed values of q^{st}, q^{diff}, U_o^{diff}, and θ. Theoretical *vs*. experimental isosteric heats of adsorption for argon on Sample B1 are shown in Fig. 11. The agreement between experimental and theoretical isosteric heats of adsorption was quite good, especially when consideration is given to the following two points.

Ideal values of α and β, the two-dimensional van der Waals' constants, were used for determining the $2\alpha/RT$ level for matching theoretical with experimental isotherms. Neglecting the polarization of the adsorbate by the surface electric field could result in an error of a few percent in V_β estimates and slightly smaller error in K' estimates for a relatively nonpolarizable adsorbate molecule such as argon (9).

As previously discussed, the uncertainty in parameter determination for the curve matching procedure is greater at low γ values. This could easily amount to a 5% error in V_β estimates.

TABLE IV

THEORETICAL ISOSTERIC HEATS OF ADSORPTION AND RELATED THERMODYNAMIC QUANTITIES FOR ARGON ADSORPTION ON SAMPLE B1 AT 77.5°K

q^{st}, kcal./mole	Θ
2.026E+00	5.791E-02
1.972E+00	7.735E-02
1.937E+00	9.227E-02
1.915E+00	1.045E-01
1.897E+00	1.155E-01
1.880E+00	1.256E-01
1.871E+00	1.339E-01
1.858E+00	1.416E-01
1.854E+00	1.487E-01
1.840E+00	1.553E-01
1.840E+00	1.618E-01
1.833E+00	1.668E-01
1.821E+00	1.725E-01
1.824E+00	1.783E-01
1.820E+00	1.825E-01
1.811E+00	1.865E-01
1.803E+00	1.916E-01
1.809E+00	1.965E-01
1.806E+00	1.999E-01

U_o^{int}, kcal./mole	U_o^{diff}, kcal./mole	q^{diff}, kcal./mole
1.001E-01	1.891E+00	1.872E+00
1.420E-01	1.817E+00	1.818E+00
1.723E-01	1.768E+00	1.783E+00
1.956E-01	1.733E+00	1.761E+00
2.154E-01	1.704E+00	1.743E+00
2.333E-01	1.677E+00	1.726E+00
2.497E-01	1.660E+00	1.717E+00
2.608E-01	1.639E+00	1.704E+00
2.752E-01	1.627E+00	1.700E+00
2.842E-01	1.607E+00	1.686E+00
2.964E-01	1.600E+00	1.686E+00
3.051E-01	1.588E+00	1.679E+00
3.123E-01	1.571E+00	1.667E+00
3.231E-01	1.568E+00	1.670E+00
3.304E-01	1.559E+00	1.666E+00
3.363E-01	1.546E+00	1.657E+00
3.428E-01	1.534E+00	1.649E+00
3.521E-01	1.534E+00	1.655E+00
3.578E-01	1.528E+00	1.652E+00

TABLE IV (Continued)

THEORETICAL ISOSTERIC HEATS OF ADSORPTION AND RELATED THERMODYNAMIC QUANTITIES FOR ARGON ADSORPTION ON SAMPLE B1 AT 77.5°K

$\underline{q}^{st}$, kcal./mole	Θ
1.794E+00	2.053E-01
1.791E+00	2.130E-01
1.791E+00	2.195E-01
1.777E+00	2.254E-01
1.776E+00	2.322E-01
1.780E+00	2.377E-01
1.773E+00	2.421E-01
1.759E+00	2.476E-01
1.765E+00	2.534E-01
1.769E+00	2.577E-01
1.765E+00	2.612E-01
1.756E+00	2.649E-01
1.744E+00	2.698E-01
1.754E+00	2.748E-01
1.758E+00	2.783E-01
1.756E+00	2.812E-01
1.751E+00	2.841E-01
1.743E+00	2.871E-01
1.730E+00	2.913E-01

$\underline{U}_{o}^{int}$, kcal./mole	$\underline{U}_{o}^{diff}$, kcal./mole	$\underline{q}^{diff}$, kcal./mole
3.626E-01	1.510E+00	1.640E+00
3.741E-01	1.500E+00	1.637E+00
3.857E-01	1.494E+00	1.637E+00
3.935E-01	1.473E+00	1.623E+00
4.035E-01	1.466E+00	1.622E+00
4.132E-01	1.465E+00	1.626E+00
4.197E-01	1.453E+00	1.619E+00
4.260E-01	1.433E+00	1.605E+00
4.356E-01	1.434E+00	1.611E+00
4.426E-01	1.433E+00	1.615E+00
4.479E-01	1.426E+00	1.611E+00
4.528E-01	1.413E+00	1.602E+00
4.583E-01	1.396E+00	1.590E+00
4.667E-01	1.401E+00	1.600E+00
4.721E-01	1.402E+00	1.604E+00
4.765E-01	1.397E+00	1.602E+00
4.804E-01	1.389E+00	1.597E+00
4.844E-01	1.377E+00	1.589E+00
4.890E-01	1.361E+00	1.576E+00

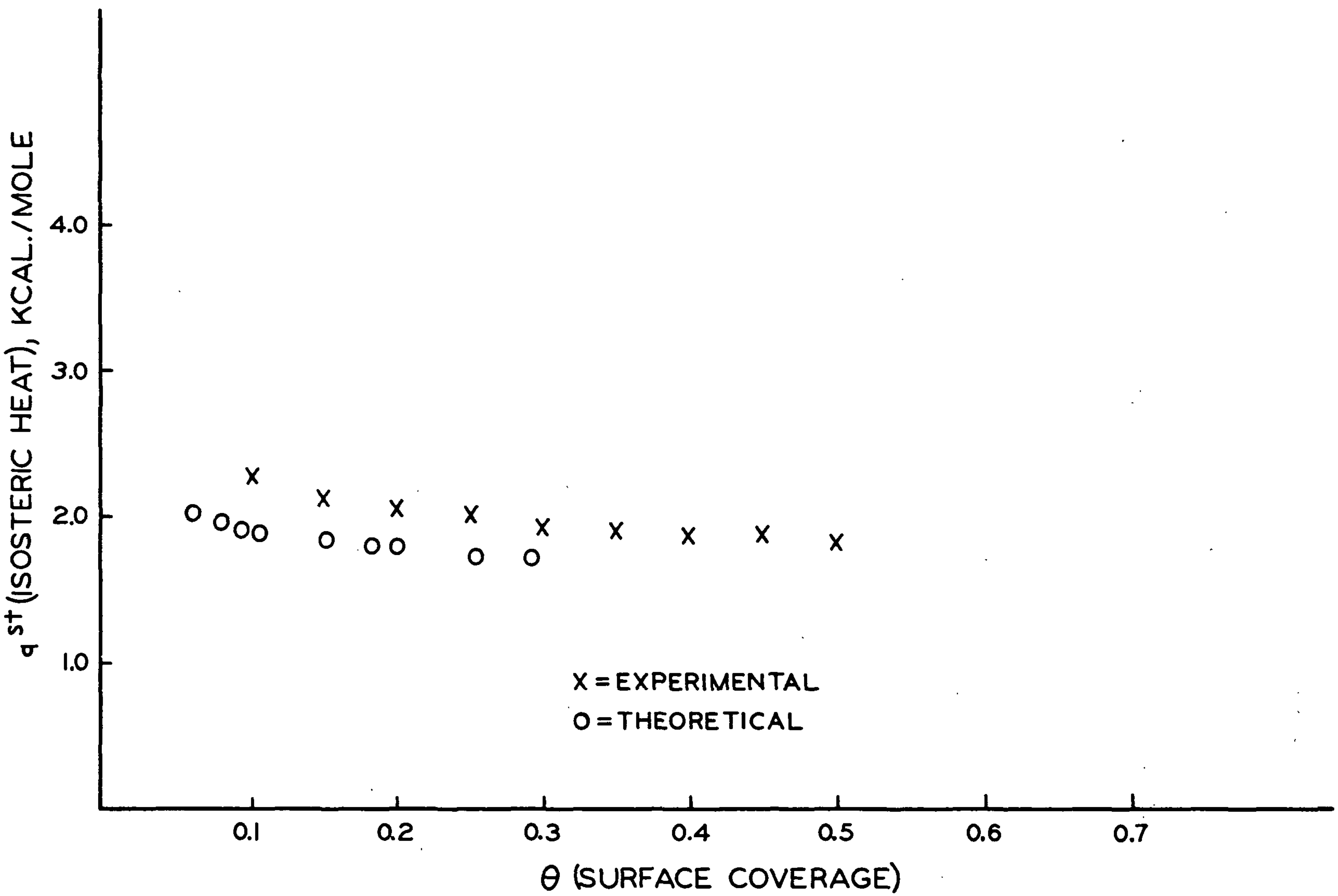

Figure 11. Theoretical and Experimental Isosteric Heats of Adsorption for Argon on Sample B1 at 77.5° and 90.1°K

Either of the above sources of error is considered sufficient to result in the observed variation between the theoretical and experimental isosteric heats of adsorption as shown in Fig. 11.

CALCULATED AND OBSERVED VALUES OF MEAN ADSORPTIVE POTENTIAL

Ross and Olivier (9) have shown that when $\Theta = 0.4$, $U_o^{diff} \cong U_o'$ for their mobile adsorption model. The isosteric heat of adsorption at $\Theta = 0.4$, $q^{st}_{\theta=0.4}$, can be obtained from experimental isotherms measured at neighboring temperatures. Values of U_o' obtained with Equation (30) are classified as (observed) U_o'.

For spherical isotropic molecules, adsorbed at low temperatures,

$$U_o' = q^{st}_{\theta=0.4} - 3R\left(\frac{T_1 \; T_2}{T_1+T_2}\right) - \frac{0.8\alpha_{id}}{\beta_{id}} \tag{30}$$

U_o' values calculated from K' estimates through the curve matching procedure are designated as (calculated) U_o'.

For argon adsorption on Sample B1 at 77.5 and 90.1°K, (calculated) $U_o' = 1.18$ kcal./mole, while (observed) $U_o' = 1.22$ kcal./mole, giving agreement to about 3.3%. Ross and Olivier (9) tabulated values of (calculated) U_o' vs. (observed) U_o' for twenty-nine adsorbents with argon, nitrogen, krypton, or oxygen as the adsorbate. The agreement between their calculated and observed U_o' values was generally within 5%.

ADSORPTION ISOTHERMS, SURFACE AREAS, AND ENERGY SITE DISTRIBUTIONS

EFFECTS OF STRUCTURAL ACCESSIBILITY ON ADSORPTION PROPERTIES

Possible effects of varying the structural accessibility of the sample on both the determined surface area and energy site distribution estimates were investigated. This was accomplished by obtaining argon adsorption isotherms on a cotton sample that had been WAN dried (Sample B3), humidified, and redried (Samples B3-H50, and B3-H86), and water dried (Sample B4). The WAN drying procedure served to develop a maximum surface area, while the humidification and redrying cycles served to close up portions of the surface. Merchant (29) has discussed the effects of humidification on the surface area of WAN dried cotton in some detail.

Solvent Exchange Dried Cotton

Argon adsorption at 77.5°K on Sample B3 is illustrated by the adsorption isotherm presented in Fig. 12. Experimental adsorption points are designated as circles, while the matching theoretical Ross and Olivier isotherm is shown as a solid line. The predicted and experimental isotherms are in good agreement. Adsorption parameters are presented in Table V. The surface was characterized as having a very broad distribution of adsorption potentials (γ = 2.0) with a mean U'_o of 1.22 kcal./mole. The solvent exchange drying procedure resulted in developing a surface area of 130 m.^{2}/g. for the cotton sample.

TABLE V

ROSS AND OLIVIER ADSORPTION PARAMETERS

	U'_o, kcal./mole	γ	$\Sigma_{R.O.}$, m.^{2}/g.
B3 WAN dried cotton	1.22	2.0	130.0
B3-H50 WAN dried cotton, humidified at 50% R.H. and redried	1.19	2.0	112.0
B3-H86 WAN dried cotton, humidified at 86% R.H. and redried	1.27	5.0	66.2
B4 water dried cotton	1.26	4.0	1.41

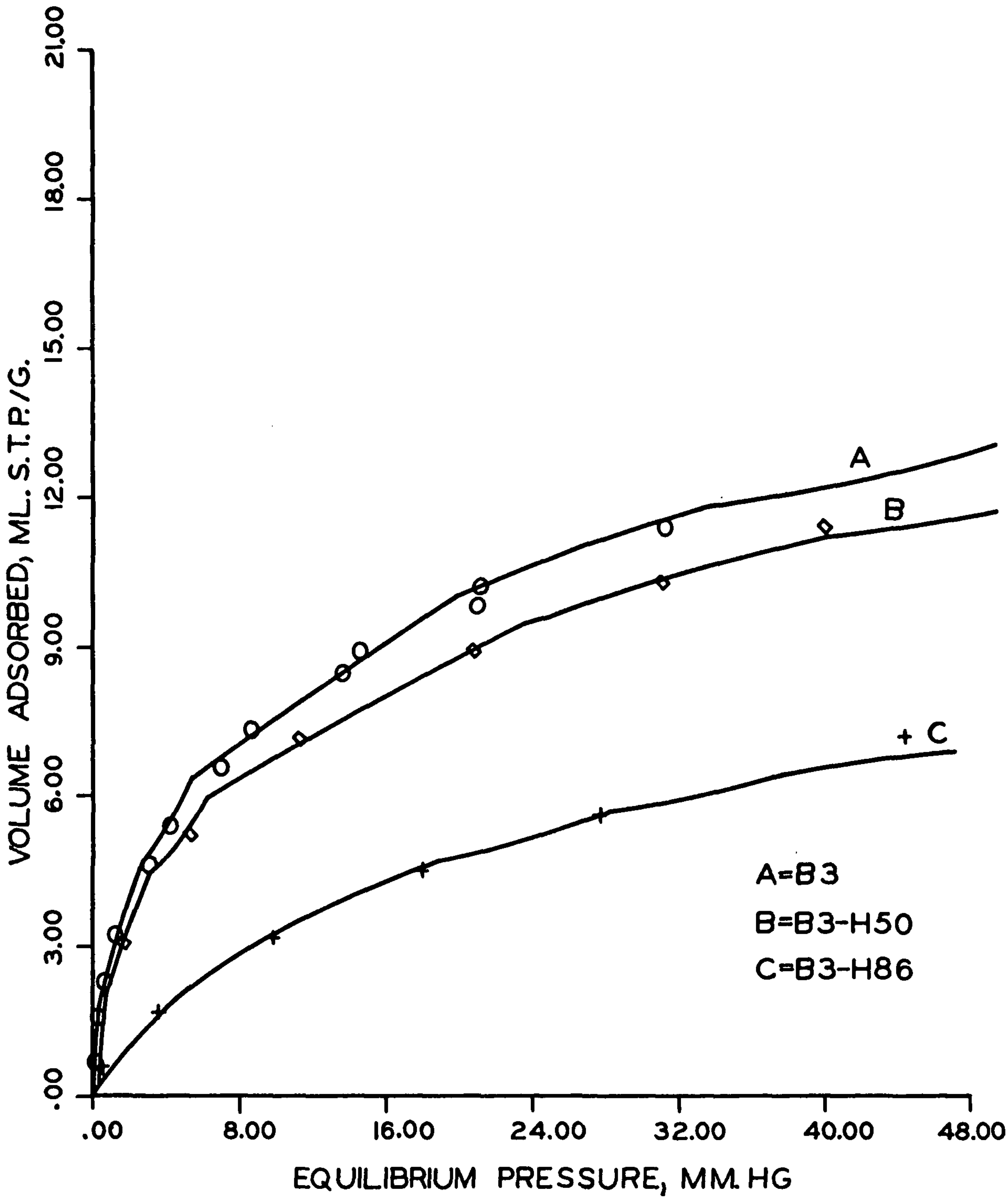

Figure 12. Theoretical and Experimental Isotherms for Argon Adsorption on Samples B3, B3-H50, and B3-H86 at 77.5°K

Surface areas in m.^{2}/g. were calculated from both Ross and Olivier theory V_β estimates and B.E.T. theory v_m estimates according to the following equations

$$\Sigma_{B.E.T.} = (v_m/22.400)(N)(\sigma_o)(10^{-20}) \qquad (30a)$$

or

$$\Sigma_{R.O.} = (V_\beta/22.400)(N)(\beta)(10^{-20}) \qquad (30b)$$

where

$\Sigma_{B.E.T.}$ = B.E.T. theory predicted surface area

$\Sigma_{R.O.}$ = Ross and Olivier theory predicted surface area

v_m = B.E.T. theory monolayer capacity estimate

N = Avogadro's number

σ_o = estimated molecular cross section of adsorbate molecule

β = two-dimensional van der Waals constant

V_β = Ross and Olivier theory monolayer capacity estimate

Irregularities may be observed for several of the model isotherms of Ross and Olivier (9). These irregularities were traced to failure to subdivide the surface into a sufficient number of homotattic patches for the numerical integration of Equation (12). When this integration was carried out more accurately, a smooth curve resulted (34).

Humidified and Redried Cotton

Theoretical and experimental isotherms for argon adsorption at 77.5°K on both B3-H50 and B3-H86 are shown in Fig. 12. Parameters obtained from the curve matching procedure are presented in Table V.

It can be seen that humidification at 50% R.H., followed by redrying, resulted in only about a 5% decrease in surface area. Both the width of the energy site distribution and the mean adsorptive potential remained the same.

Humidification at 86% R.H., followed by redrying, decreased the surface area by almost 50%. A slight increase in the adsorptive potential and a significant decrease in the width of the range of the adsorptive potential was noted. This shift of the determined energy site distribution probably resulted from the elimination of low energy sites present in small pores that were sealed off by the humidification and drying procedure. The decrease in surface area is attributable to increased bonding in the microstructure as a result of capillary forces.

Water Dried Cotton

Parameters for argon adsorption at 77.5°K on Sample B4 are given in Table V, and the theoretical and experimental isotherms are shown in Fig. 13. It can be seen that drying from water greatly decreased the available surface area of the cotton. Values of $\underline{U}_o'$ and γ for Sample B4 were nearly identical to the corresponding values for Sample B3-H86. This indicates that the closing of larger pores and the increasing of fibrillar bonding did not affect the energy site distribution even though the sample exhibited only about one percent of the surface area of the WAN dried sample.

The results of the argon adsorption runs on Sample B3, B3-H50, B3-H86, and B4 indicate that the energy site distribution of cotton cellulose is rather independent of the surface area available. This may be interpreted to mean that cellulose surfaces, regardless of their location within the cotton fiber structure, exhibit similar distributions of adsorptive potentials. These distributions are characterized as being very broad with a low mean adsorptive potential.

Stamm and Tarkow (35), based on the observations of Stamm and Hansen (36), proposed that during the solvent exchange procedure nonpolar liquids would replace all but a monolayer of the intermediate polar liquid. Merchant (29) disagreed with the proposal of Stamm and Tarkow since he found less residual polar liquid

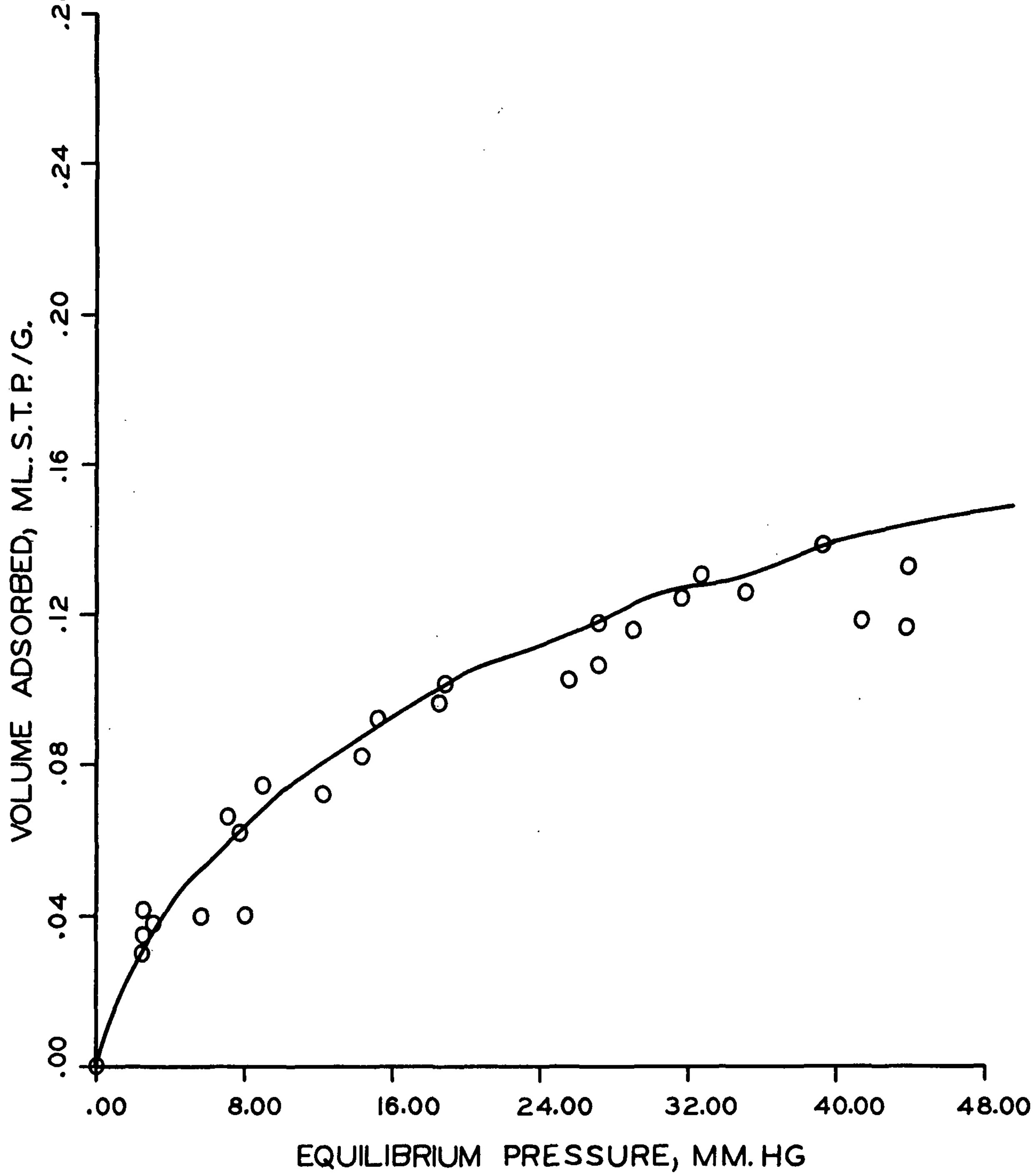

Figure 13. Theoretical and Experimental Isotherms for Argon Adsorption on Sample B4 at 77.5°K

for higher surface area samples. Merchant (29) proposed that the residual liquid was mechanically entrapped and sealed in pores in the fiber structure.

Merchant (29) showed that moistening a solvent exchange dried sample released the entrapped or adsorbed residual liquids. Humidification and drying, at a humidity level high enough to cause a decrease in surface area, would also be expected to remove residual exchange liquids.

In the present study, no large change in the distribution of adsorptive potentials was observed either after humidification and redrying or as a result of water drying. These results lend strong support to Merchant's conclusion (29) that the residual exchange liquid is entrapped mechanically and leaves considerable doubt as to the possibility of an unreplaced monolayer of polar liquid as claimed by Stamm and Tarkow (35).

EFFECTS OF CHEMICAL MODIFICATION ON ADSORPTION PROPERTIES

Possible effects of chemical modification of the cellulose surface on the energy site distribution of the surface were investigated by obtaining and analyzing argon adsorption isotherms for three samples of varying chemical composition.

Oxidized Cotton

Sample BO-1, periodate oxidized cotton, was solvent exchanged and dried as described in the Appendix. A total of 0.136 g. of oxygen were consumed per gram of cellulose, resulting in a highly oxidized sample.

Theoretical and experimental isotherms for argon adsorption at 77.5°K on Sample BO-1 are shown in Fig. 14. Determined adsorption parameters are listed in Table VI.

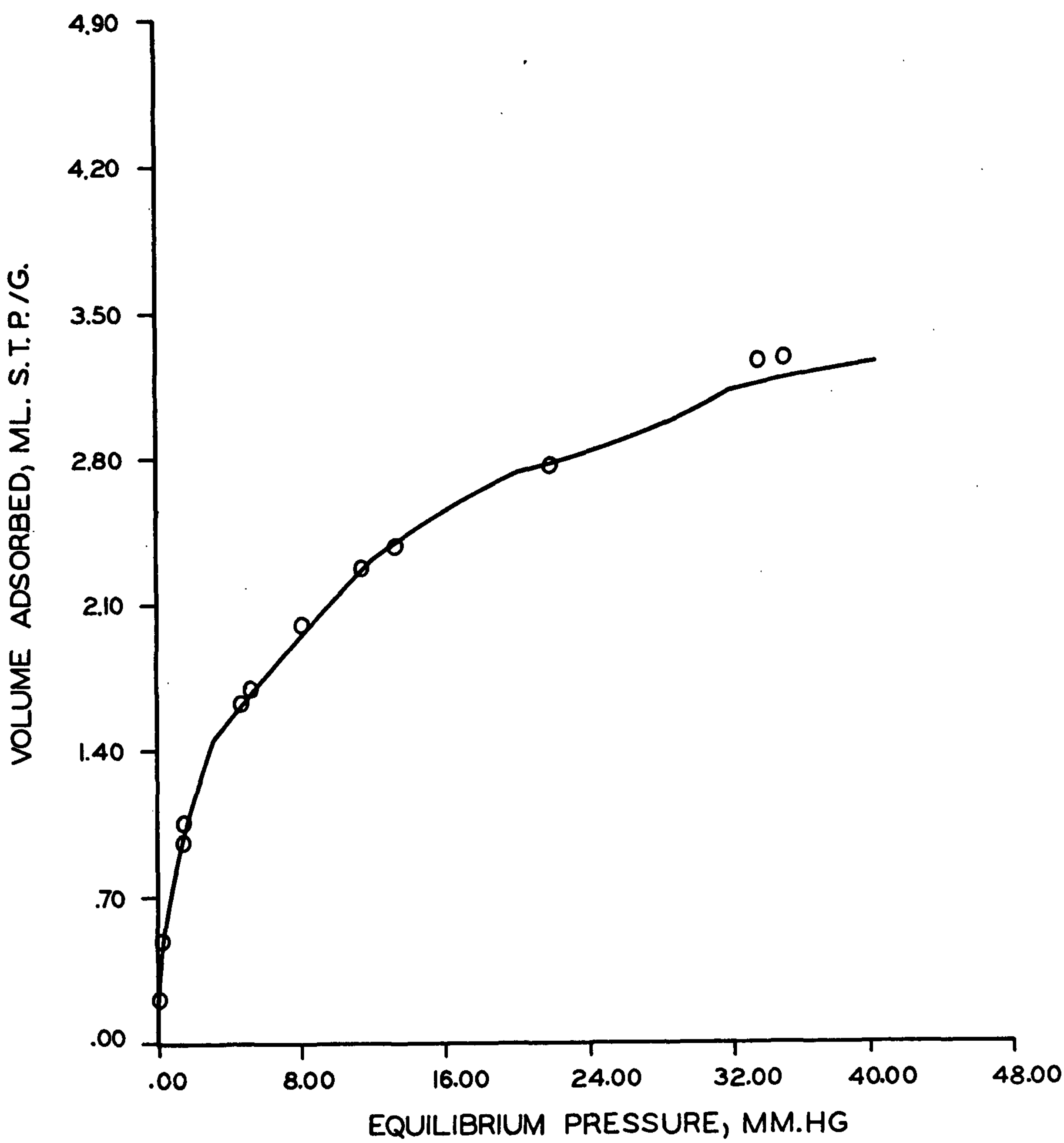

Figure 14. Theoretical and Experimental Isotherms for Argon Adsorption on Sample BO-1 at 77.5°K

TABLE VI

ROSS AND OLIVIER ADSORPTION PARAMETERS

Adsorbent	$\underline{U}_o'$, kcal./mole	γ	$\Sigma_{R.O.}$, m.^{2}/g.
BO-1 WAN dried oxidized cotton	1.29	2.0	31.0
BHOLO-1 incense cedar holocellulose	1.10	5.0	0.52
BHYD-1 hydroxyethylated cotton combers	1.17	3.0	1.36

A small increase in $\underline{U}_o'$, the mean adsorptive potential, was observed for the oxidized cellulose (BO-1) over unoxidized cellulose (B3). The width of the range of adsorptive potentials remained the same, however. The increased carboxyl content of the surface may have led to greater polarization of argon molecules. However, since no estimates of the surface electric field strengths of cellulose or oxidized cellulose are available, it is not possible to discuss this topic in more detail. The WAN dried oxidized cellulose developed only about one-fourth the surface area of normal WAN dried cotton. This may have in part been due to the removal of exterior fibrils during oxidation. The oxidation also may have reduced the attraction between the surface and water or methanol, thereby decreasing the degree of initial swelling. (Since periodate oxidized cellulose is cross-linked, this may also have reduced initial swelling.) This would be expected since alcohols are more soluble in water than the corresponding aldehydes.

<u>Hydroxyethylated Cotton Combers</u>

Theoretical and experimental isotherms for argon adsorption at 77.5°K on Sample BHYD-1 are shown in Fig. 15. Good agreement was obtained between the model and experimental isotherms. Determined adsorption parameters are presented in Table VI. It is apparent that hydroxyethylation resulted in a significant lowering of the mean adsorptive potential exhibited by the sample. Little change in the width of the distribution was noted.

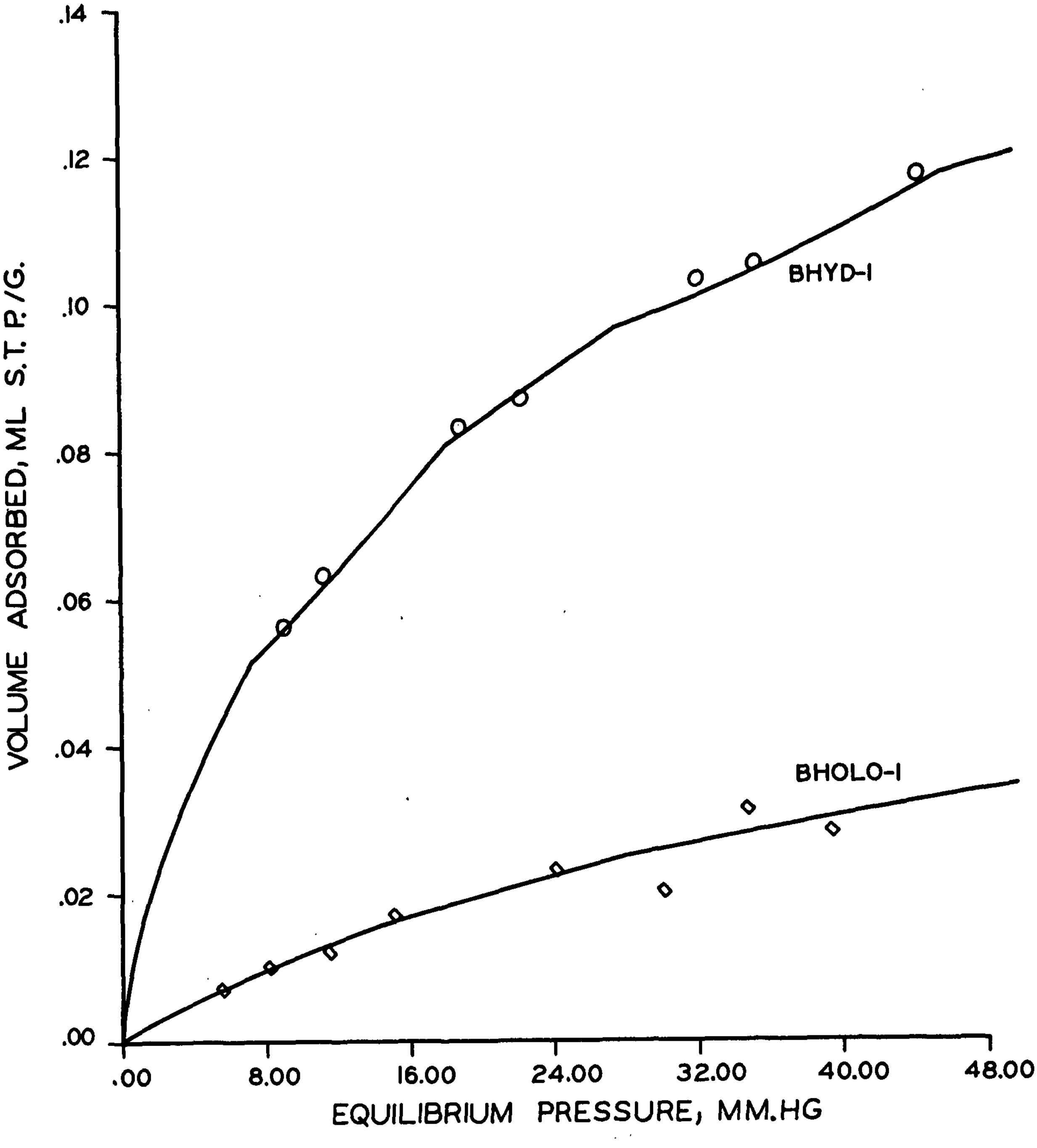

Figure 15. Theoretical and Experimental Isotherms for Argon Adsorption on Samples BHYD-1, and BHOLO-1 at 77.5°K

Holocellulose

Theoretical and experimental isotherms for the adsorption of argon on BHOLO-1 at 77.5°K are also presented in Fig. 15. Adsorption parameters are listed in Table VI. The holocellulose surface was characterized by a low mean adsorptive potential and a wide range of adsorptive potentials. The U'_o value was significantly lower than that for cotton. The presence of hemicelluloses may be the reason for the observed low U'_o. Results of chemical analysis of BHOLO-1 are given in the Appendix in Table XX.

DISCREPANCIES BETWEEN ROSS AND OLIVIER AND B.E.T. ESTIMATES OF SURFACE AREA

In their monograph, Ross and Olivier (9) compared V_β estimates (monolayer capacity estimates from Ross and Olivier theory) with v_m estimates (monolayer capacity estimates from B.E.T. or point B method) for almost thirty adsorbents. Generally, the agreement between V_β and v_m estimates was within 15%. However, for two adsorbents, rutile and diamond dust, the V_β estimates were considerably greater than the corresponding v_m estimates. Both of these adsorbents were characterized as exhibiting mean adsorptive potentials lower than those listed for the other adsorbents. Gregg and Sing (16) have, in general, commented favorably on the efforts of Ross and Olivier but have expressed concern for the discrepancies observed between B.E.T. and Ross and Olivier (9) monolayer capacity estimates for both rutile and diamond dust.

GAS ADSORPTION, GEOMETRIC, AND ELECTRICAL SURFACE AREA ESTIMATES

Cellulosic Adsorbents

Two samples of rayon fibers were selected to permit geometric and gas adsorption surface area determinations on each sample. Calculations of geometrical surface areas for Samples B5-RAY and B6-RAY are given in the Appendix in Tables XXI and XXII.

Theoretical and experimental isotherms for argon adsorption at 77.5°K on both B5-RAY and B6-RAY are shown in Fig. 16 and 17. Geometric, Ross and Olivier (9), and B.E.T. surface area estimates are given in Table VII.

TABLE VII

GAS ADSORPTION AND GEOMETRIC SURFACE AREA ESTIMATES

Adsorbent	Σ_{GEO}, m.^{2}/g.	$\Sigma_{B.E.T.}$, m.^{2}/g.	$\Sigma_{R.O.}$, m.^{2}/g.	U_o', kcal./mole	γ
B5-RAY water-dried rayon	0.342	0.176	0.472	1.32	5
B6-RAY water-dried high tenacity rayon	0.252	0.181	0.422	1.38	7

From the above experimental results, it is obvious that the B.E.T. estimates of surface area are grossly in error. A valid gas adsorption surface area should be greater than the corresponding geometric surface area since the adsorbate molecules are "seeing" the solid structure on a molecular scale. The Ross and Olivier surface area estimates satisfy this condition. It also should be made clear that the geometric surface area estimates of Table VII represent minimum values. Electron photomicrographs of both the normal viscose and high tenacity viscose rayon exhibited considerable fine surface roughness. Although circular in cross section, the high tenacity rayon fibers appeared to have a considerably rougher fine surface structure than the normal viscose rayon fibers.

Since the surface of B6-RAY was rougher than that of B5-RAY, one would assume

$$\frac{\Sigma_{geo,B6}}{\Sigma_{real,B6}} < \frac{\Sigma_{geo,B5}}{\Sigma_{real,B5}} \qquad (31)$$

When Ross and Olivier area estimates are assumed to be "real" areas, we obtain

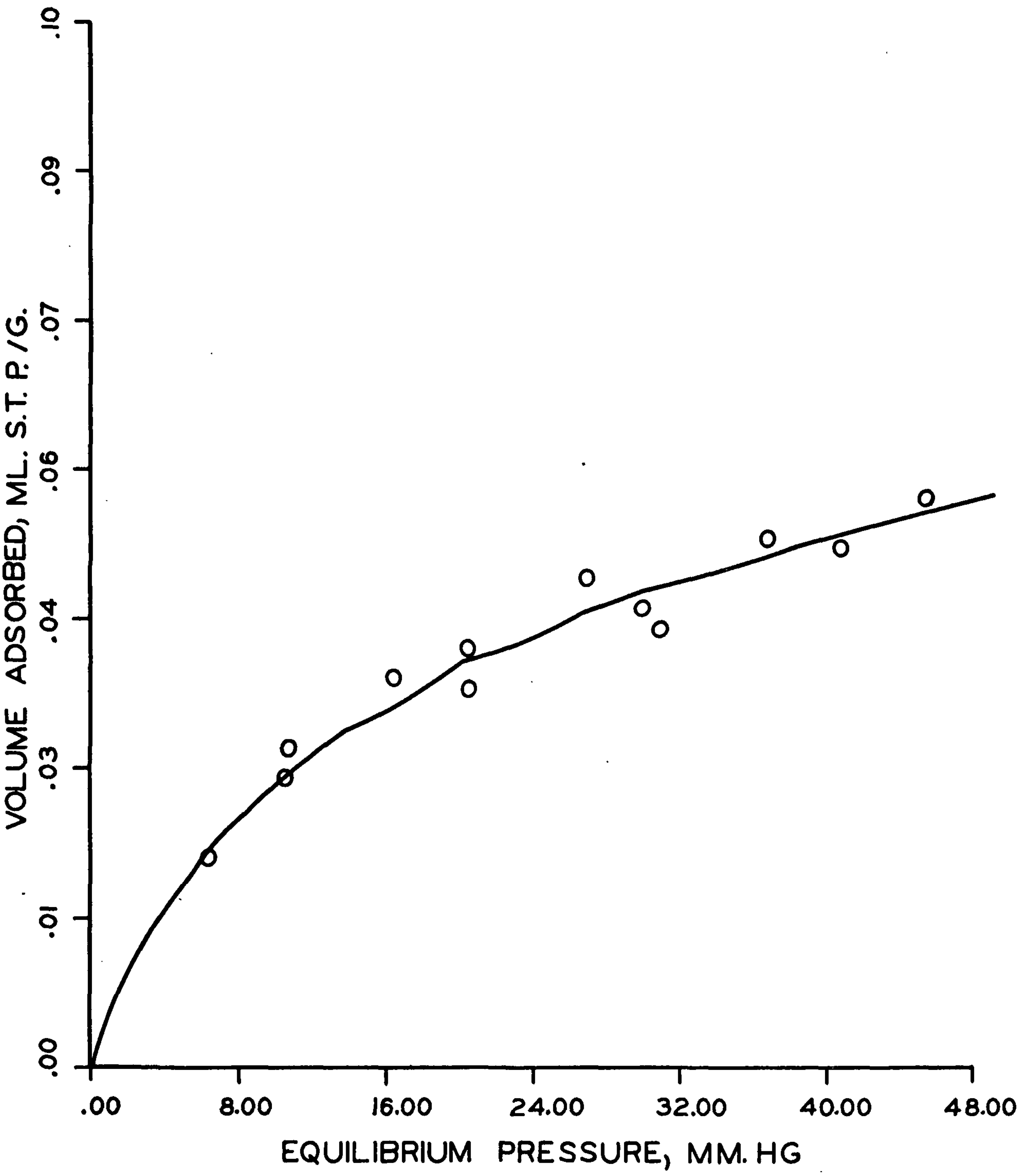

Figure 16. Theoretical and Experimental Isotherms for Argon Adsorption on Sample B5-RAY at 77.5°K

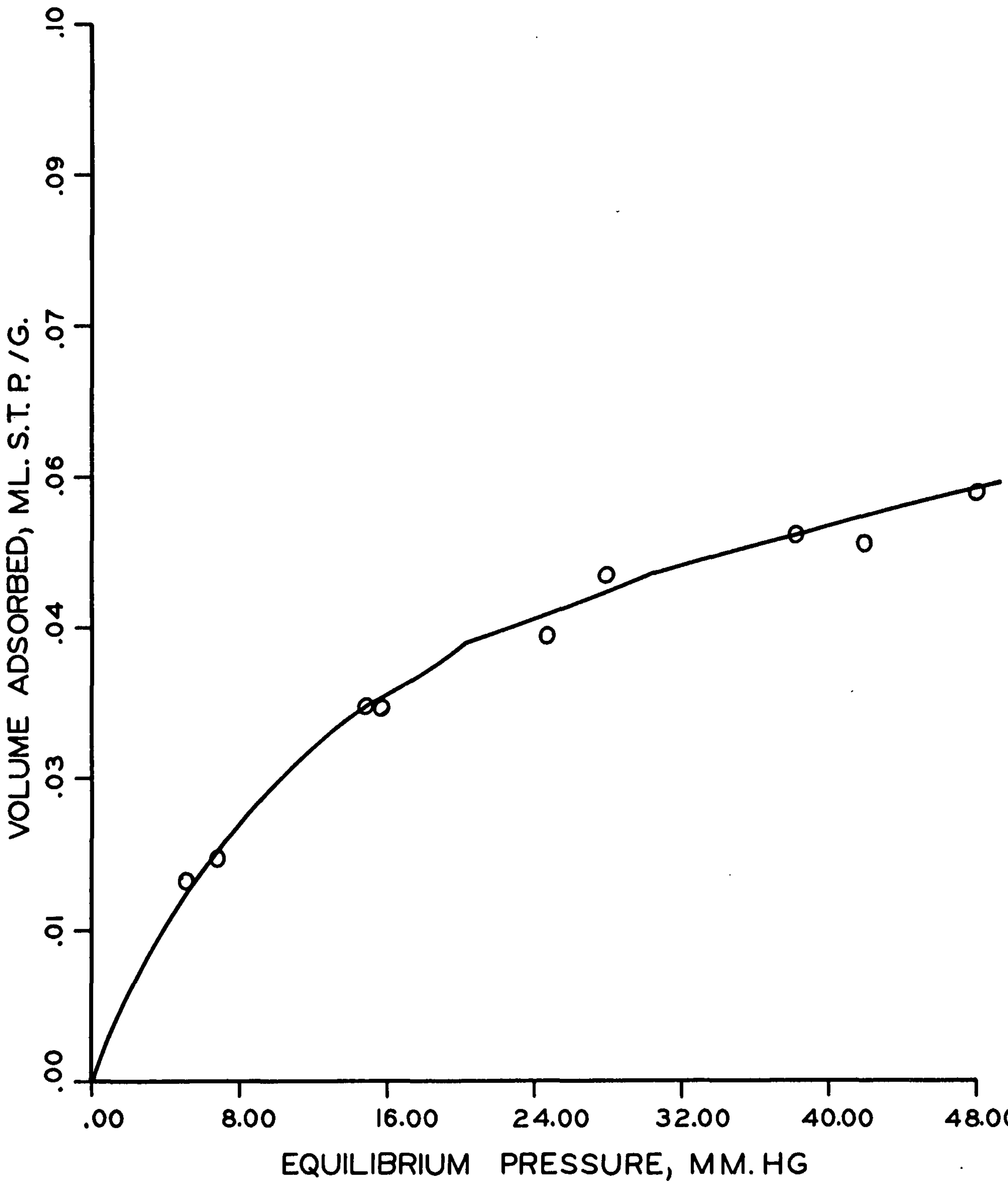

Figure 17. Theoretical and Experimental Isotherms for Argon Adsorption on Sample B6-RAY at 77.5°K

$$\frac{0.252}{0.422} < \frac{0.342}{0.472} \quad \text{or} \quad 0.598 < 0.725$$

thereby lending support to the above assumption.

When the corresponding B.E.T. areas are considered, one obtains

$$\frac{\sum_{geo,B6}}{\sum_{B.E.T.,B6}} < \frac{\sum_{geo,B5}}{\sum_{B.E.T.,B5}} \tag{32}$$

since

$$\frac{0.252}{0.181} < \frac{0.342}{0.176} \quad \text{or} \quad 1.39 < 1.94$$

which is also consistent with the original assumption. The fact that the magnitude of variation for the two sets of inequalities differs can be explained by the fact that the mean adsorptive potential, $\underset{\sim}{U'_o}$, for B6-RAY was greater than that for B5-RAY as shown in Table VII. The effect of the $\underset{\sim}{U'_o}$ value on the ratio $\sum_{R.O.}/\sum_{B.E.T.}$ is discussed in a later section.

It should be made clear that possible fiber to fiber bonding of the rayon did not result in a reduction of the available surface area. Sorptometer measurements on untreated and water-dried rayon could not detect any surface area changes due to bonding (0.394 $m.^2/g.$ untreated, 0.390 $m.^2/g.$ water dried). This was expected since rayon fibers are rather stiff and nondeformable, are without lumens, and, therefore, would not likely develop significant bonded area.

Previously, Ingmanson and Thode (37) determined the surface area of a softwood bleached sulfite pulp by geometric measurements, silvering technique, and filtration resistance. They found good agreement among the three methods, all of which produced areas of about 0.75 $m.^2/g.$ for classified pulp. Swanson and Steber (38) found a B.E.T. area of 0.64 $m.^2/g.$ for classified softwood bleached sulfite handsheets.

A bonded area of 0.04 m.^{2}/g. was determined, thereby indicating an unbonded area of about 0.72 m.^{2}/g. which is in good agreement with the results of Ingmanson and Thode.

The above results are quite surprising and contrary to requirement that the gas adsorption area be larger than the geometric area as discussed previously. These results can be explained with consideration of the following:

For Sample B5-RAY, the B.E.T. area was only one-half the geometric area, while for the pulp sample (37, 38), the two estimates were approximately the same.

$$\Sigma_{B.E.T.,B5} / \Sigma_{geo,B5} \simeq 0.5 \qquad (33)$$

while

$$\Sigma_{B.E.T.,\ pulp} / \Sigma_{geo,pulp} \simeq 1.0.$$

These results can at least partially be explained in terms of microscopic surface roughness. The microscopic surface roughness of the pulp fibers is considerably greater than that for rayon fibers due to the presence of pits, fibrils, etc. This would mean that the geometric area estimate for the pulp fibers would be relatively more in error (lower) than that for the rayon fibers.

Then since

$$\frac{\Sigma_{geo,pulp}}{\Sigma_{real,pulp}} < \frac{\Sigma_{geo,B5}}{\Sigma_{real,B5}} \qquad (34)$$

it follows that

$$\frac{\Sigma_{B.E.T.,pulp}}{\Sigma_{geo,pulp}} > \frac{\Sigma_{B.E.T.,B6}}{\Sigma_{geo,B6}} \qquad (35)$$

The inequality (34) was observed experimentally. These results lend more support to the finding that the B.E.T. theory predicts incorrect surface areas for cellulose adsorbents.

Noncellulosic Adsorbents

Silver Iodide

Van den Hul (39) carried out a thorough investigation of both the capacitance (40) and the negative adsorption methods (41) for determining the specific surface areas of solids suspended in a liquid. He obtained B.E.T. area estimates from argon adsorption, hydrodynamic area estimates, and surface area estimates based on observations using an optical microscope for silver iodide particles.

For eight different samples, he consistently obtained good agreement between surface area estimates based on the negative adsorption and capacitance methods. The ratios (average area estimates from electrical measurements/B.E.T. areas) varied from 2.9 to 3.85.

Making use of an argon isotherm presented in Van den Hul's thesis (39), it was possible to determine Ross and Olivier (9) parameters for the AgI surface. The results are summarized in Fig. 18 and Table VIII. The surface exhibited a low mean adsorptive potential (U'_o = 1.14 kcal./mole) and a γ value (1.50) characteristic of a very heterogeneous surface. The ratio of $\Sigma_{R.O.}/\Sigma_{B.E.T.}$ was calculated to be 2.70. The surface area obtained from the Ross and Olivier (9) V_β estimate was in good agreement with Van den Hul's (39) estimate obtained by both the negative adsorption and capacitance methods.

Van den Hul (39) originally explained the discrepancy between B.E.T. and electrochemical areas of AgI samples on the assumption that aggregation occurred during drying. This explanation seems rather unlikely, especially for a crystalline, nondeformable substance. It appears more likely that the B.E.T. estimates were seriously in error due to both the low mean adsorptive potential and high surface heterogeneity characteristic of the surface of AgI.

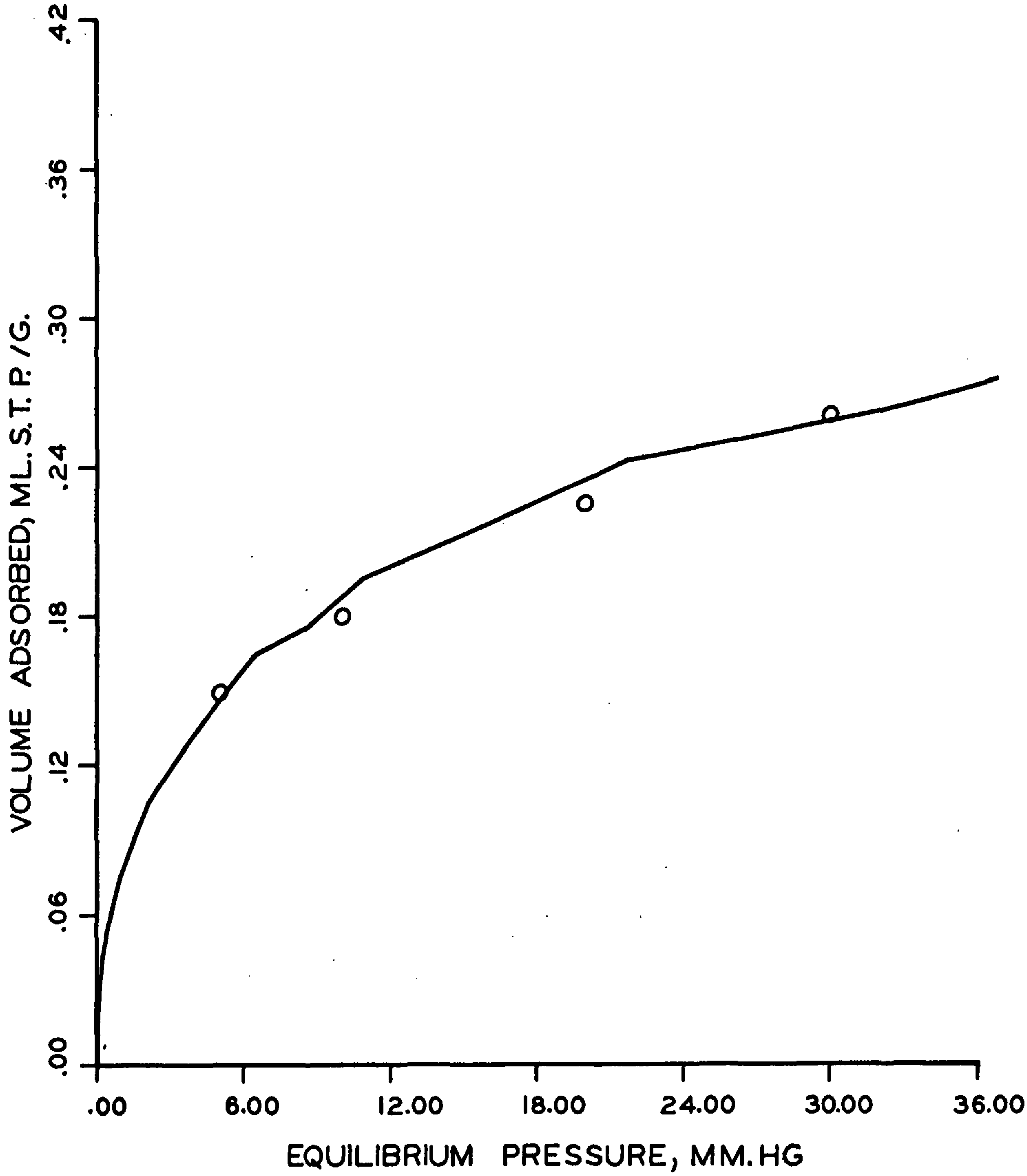

Figure 18. Theoretical and Experimental Isotherms for Argon Adsorption on Silver Iodide [Experimental Data of Van den Hul (39)]

TABLE VIII

SILVER IODIDE SURFACE AREA ESTIMATES

Method	Surface Area, $m.^2/g.$
Argon adsorption B.E.T. analysis	1.00
Argon adsorption Ross and Olivier analysis	3.27
Capacitance (40)	3.7
Negative adsorption (41)	3.3

Titanium Dioxide

The supply of the titanium dioxide for the gas adsorption study had been previously characterized by Williams and Webb (33), who obtained surface area estimates by sedimentation measurements and optical measurements. Williams obtained surface area estimates from 11.8 to 12.6 $m.^2/g.$ based on sedimentation data. Webb, who measured 1295 particles and assumed spherical shape, calculated the number average surface area to be 12.73 $m.^2/g. \pm 0.18$ $m.^2/g.$ at the 95% confidence level.

Argon adsorption on B-TiO_2 at 77.5°K is represented by the theoretical and experimental isotherms shown in Fig. 19. The surface was characterized as being heterogeneous ($\gamma = 1.0$) and exhibiting a low mean adsorptive potential ($\underline{U}'_o = 1.29$ kcal./mole).

B.E.T. analysis of the data resulted in a surface area estimate of 7.1 $m.^2/g.$, while the Ross and Olivier (9) surface area estimate was 22.7 $m.^2/g.$ This represents another clear case where the B.E.T. estimate of surface area is grossly in error, since it is considerably less than the geometric surface area estimate. Again, the reported geometric surface area must be considered as a minimum estimate since considerable fine surface roughness was present but not considered in the calculations. The Ross and Olivier area estimate is again reasonable.

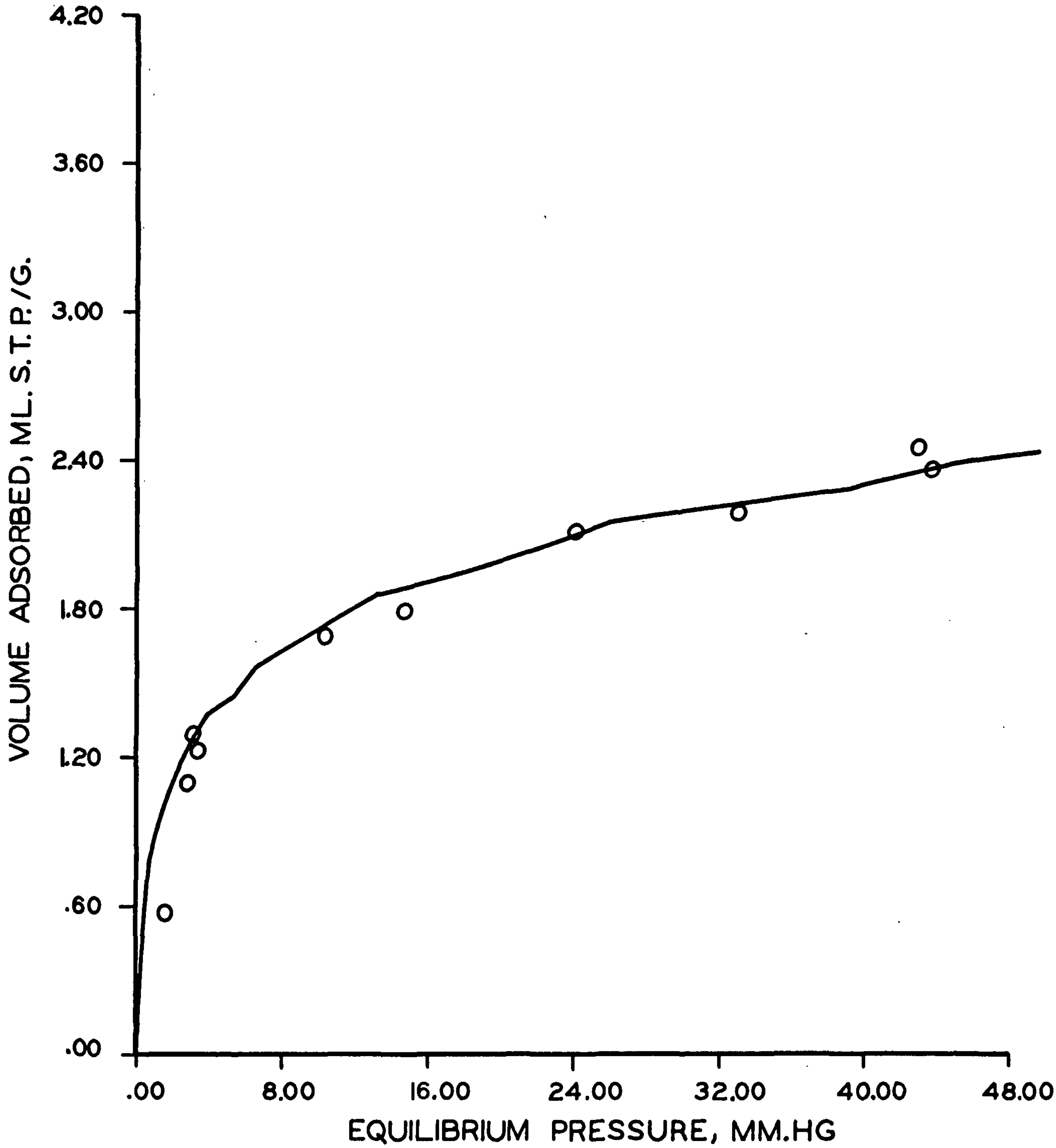

Figure 19. Theoretical and Experimental Isotherms for Argon Adsorption on Sample B-TiO_2 at 77.5°K

Teflon "6"

Whalen (42) determined geometric and B.E.T. surface areas for Teflon "6" to be 15.4 and 15.2 m.^{2}/g. Shadowed particles were viewed rather than surface replicas for the geometric area estimate, and consideration was not given to surface roughness. Argon adsorption data at 77.5°K were used for the B.E.T. calculation.

Using the data of Whalen, Ross and Olivier analysis was carried out. Theoretical and experimental isotherms are shown in Fig. 20. The Ross and Olivier approach gave a surface area estimate of 24.8 m.^{2}/g. Again, the Ross and Olivier method has predicted a surface area estimate more realistic than that of the B.E.T. theory.

VARIATION OF THE RATIO (ROSS AND OLIVIER AREA/B.E.T. AREA) AS A FUNCTION OF ADSORPTIVE POTENTIAL

In the previous section, it has been demonstrated that the B.E.T. theory provided inaccurate surface area estimates for a number of low adsorptive potential adsorbents.

Table IX represents a summary of completed experimental adsorption analyses and, in addition, the results of analyses of certain pertinent literature data. Of major interest is the quantity $\Sigma_{R.O.}/\Sigma_{B.E.T.}$, the ratio of Ross and Olivier (9) area to the B.E.T. area for a given sample. It is immediately obvious that the ratio $\Sigma_{R.O.}/\Sigma_{B.E.T.}$ is by no means constant for the samples under discussion. An apparent correlation exists, however, between the mean adsorptive potential, $\underline{U}'_o$, and the ratio $\Sigma_{R.O.}/\Sigma_{B.E.T.}$ for a given sample. This is demonstrated by Fig. 21 which exhibits the dependence of the ratio $\Sigma_{R.O.}/\Sigma_{B.E.T.}$ (or in some cases $\Sigma_{R.O.}/\Sigma_{pt.B}$) on $\underline{U}'_o$. The results of the present work are seen to be in good agreement with the findings of Ross and Olivier (9), which clearly show increasing discrepancies between $\Sigma_{R.O.}$ and $\Sigma_{pt.B}$ estimates for samples with decreasing mean adsorptive potentials. It is also interesting to note that, in general, for samples with a $\underline{U}'_o$ value greater

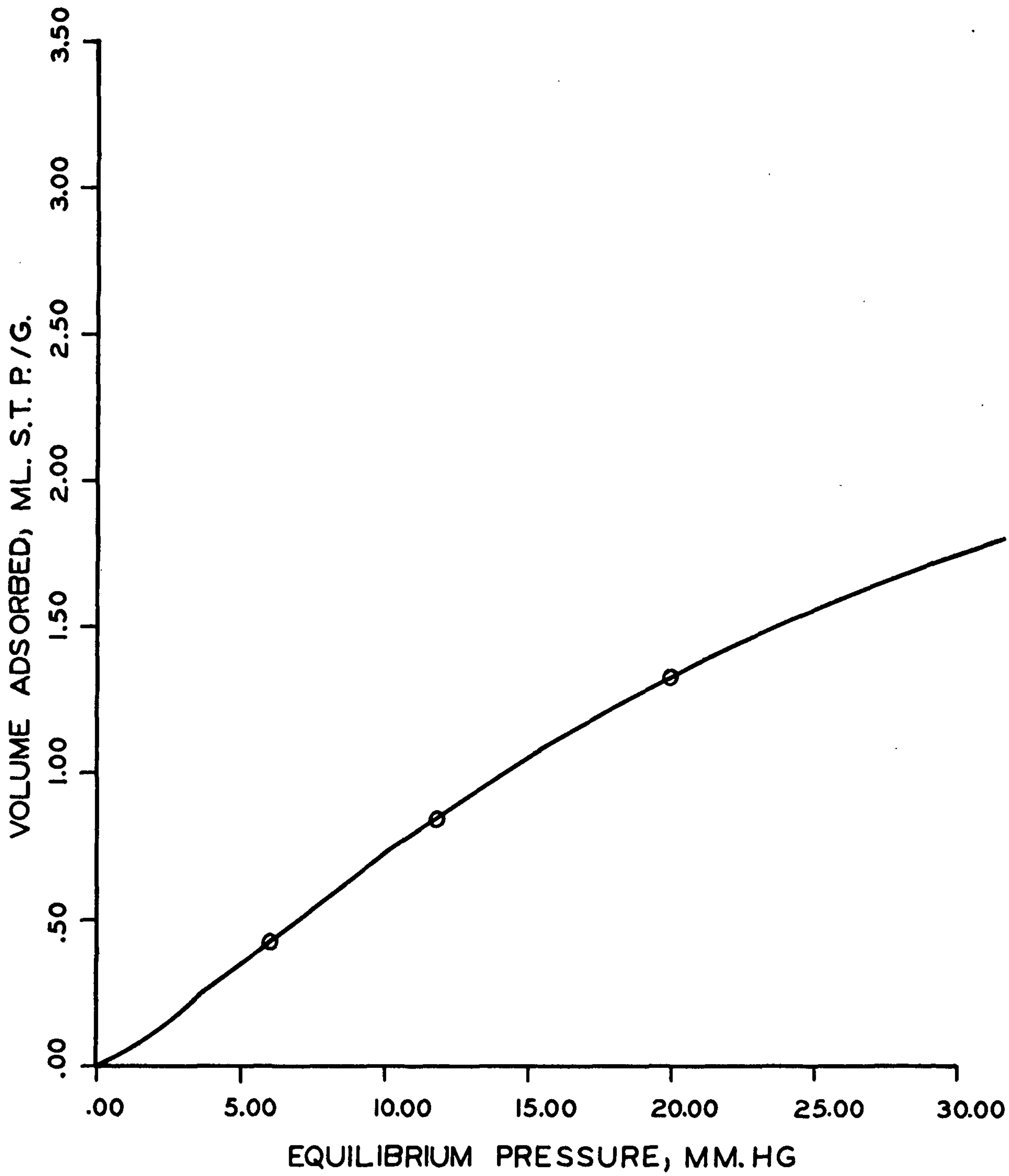

Figure 20. Theoretical and Experimental Isotherms for Argon Adsorption on Teflon "6" [Experimental Data of Whalen, et al. (42)]

TABLE IX

SUMMARY OF EXPERIMENTAL RESULTS

Adsorbent	$\Sigma_{B.E.T.}$, m.^{2}/g.	Σ_{GEO}, m.^{2}/g.	$\Sigma_{R.O.}$, m.^{2}/g.	U'_o, kcal./mole	γ	$\Sigma_{R.O.}/\Sigma_{B.E.T.}$
B3 WAN dried cotton	44.6	--	130.0	1.22	2.0	2.92
B3-H50 WAN dried cotton, humidified at 50% R.H.	41.2	--	123.0	1.19	2.0	2.99
B3-H76 WAN dried cotton, humidified at 76% R.H.	22.6	--	66.2	1.27	5.0	2.93
B4 water-dried cotton	0.486	--	1.41	1.26	4.0	2.91
BO-1 WAN dried periodate oxidized cotton	10.7	--	31.0	1.29	2.0	2.90
B5-RAY water-dried rayon	0.176[a] 0.394[b]	0.342	0.472	1.32	5.0	2.69[a]
B6-RAY water-dried, high tenacity rayon	0.181	0.252	0.422	1.38	7.0	2.25
BHYD-1 water-dried hydroxy-ethylated cotton combers	0.377	--	1.36	1.17	3.0	3.61
BHOLO-1 incense cedar chlorite holocellulose	0.131	--	0.52	1.10	5.0	3.97
B1$_{77.5}$ WAN dried cotton, adsorption at 77.5°K	41.4	--	135.0	1.18	2.0	3.26

See end of table for footnotes.

TABLE IX (Continued)

SUMMARY OF EXPERIMENTAL RESULTS

Adsorbent	$\Sigma_{B.E.T.}$, m.^{2}/g.	Σ_{GEO}, m.^{2}/g.	$\Sigma_{R.O.}$, m.^{2}/g.	$\underline{U}'_o$, kcal./mole	γ	$\Sigma_{R.O.}/\Sigma_{B.E.T.}$
$Bl_{90.1}$ WAN dried cotton, adsorption at 90.1°K	38.8[d]	--	112.0	1.17	1.85[c]	2.89
Teflon "6", sample of Whalen (42)	9.0[e]					2.60
	11.9[f]					1.96
	15.2[g]	15.4[h]	23.4	1.26	10.0	1.54
Silver iodide, sample of Van den Hul	3.3[i]	3.3[i]				
	3.7[j]	3.7[j]				
	0.883	0.88	3.27	1.14	1.50	3.70
Titanium dioxide	7.1	12.73	22.7	1.29	1.0	3.20

---

[a]B.E.T. apparatus.

[b]Sorptometer.

[c]γ Corrected to 77.5°K.

[d]Using 15.5 A.°^{2}/molecule, at 90.1°K.

[e]Chessick (10).

[f]Whalen, N_2 — maximum estimates (42).

[g]Whalen, Ar (42).

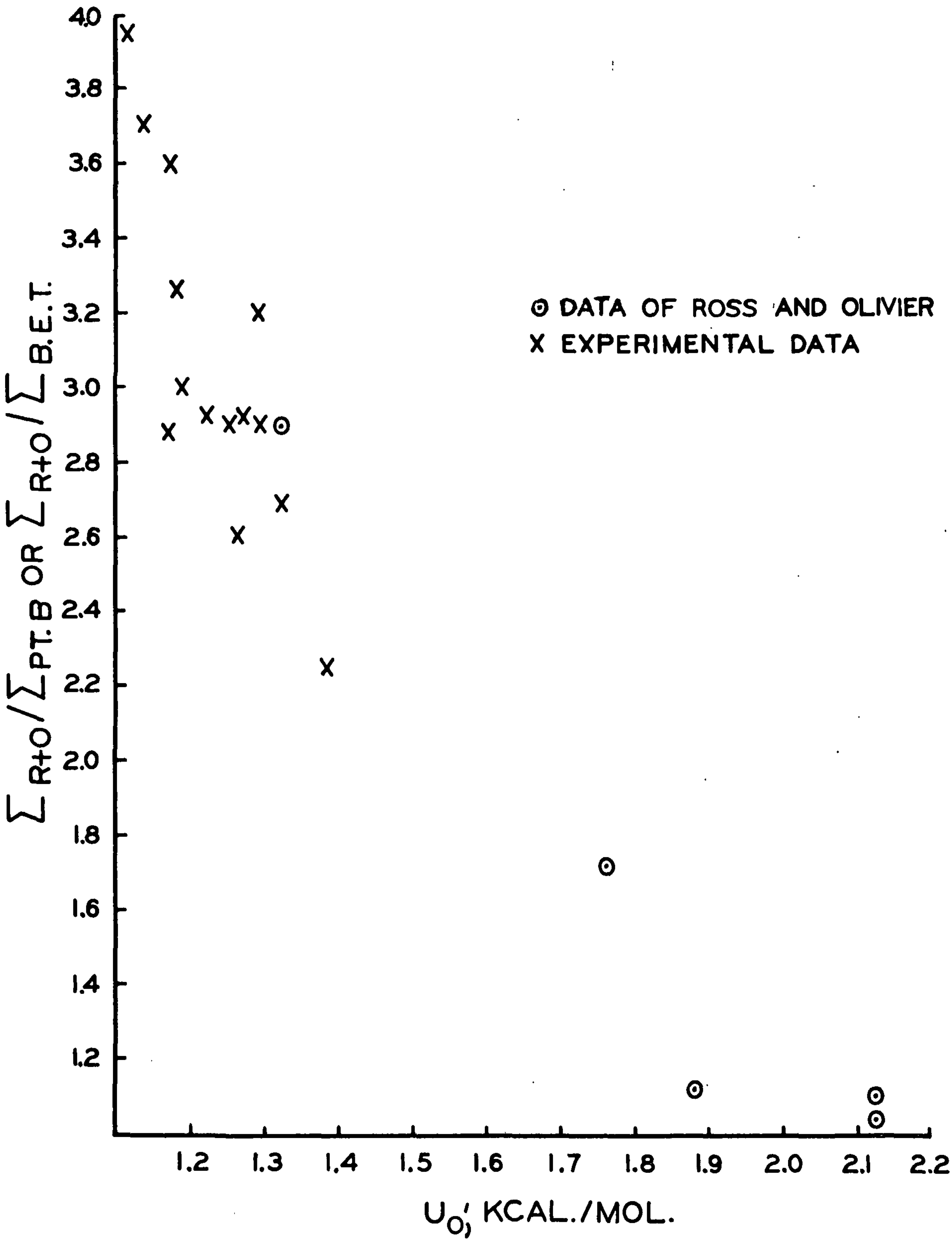

Figure 21. Variation of the Ratios $\Sigma_{\underline{R}+0}/\Sigma_{Pt.B}$ and $\Sigma_{\underline{R}+0}/\Sigma_{B.E.T.}$ with Mean Adsorptive Potential for Argon Adsorption on Several Samples at 77.5°K

than 2.10 kcal./mole, the agreement between $\sum_{R.O.}$ and $\sum_{B.E.T.}$ or $\sum_{R.O.}$ and $\sum_{pt.B}$ estimates was within 10%.

In their discussion of argon adsorption on diamond dust, Ross and Olivier (9) have attempted to explain the large discrepancies between v_m and V_β estimates on the basis of the low U_o' value (1.32 kcal./mole) observed for the diamond dust-argon system according to the following:

> "The immediate practical result of the low adsorptive potentials is that the specific area of the dust determined by the B.E.T. method is grossly in error. The part of the surface having an adsorptive potential less than that of the liquid adsorbate remains sparsely occupied, even as multilayers build up over the more energetic patches of the surface; this effect combined with that produced by a low value of γ (3.0) leads to a value of v_m by the B.E.T. method that is about one-third of the value of V_β."

The above appeared to represent a valid argument but unfortunately was not supported with the necessary data, namely the adsorptive potential of the liquid adsorbate in conjunction with the energy site distribution curve. In the present study, experimental isosteric heats of adsorption were determined for argon adsorption on Sample B1 (see Table V). Experimental differential heats of adsorption were obtained by Equation (29) and are listed in Table X. Theoretical differential adsorptive potentials ($U_{o_{diff}}$) were calculated and listed in Table IV. The heat of liquefaction for argon is 1.50 kcal./mole. At a surface coverage of $\theta = 0.35$, the experimental differential heat of adsorption was about 1.76 kcal./mole. From the results of the model calculations shown in Table IV, it can be seen that, as $U_{o_{diff}}$ decreased from 1.89 to 1.36 kcal./mole, Q_{diff} decreased from 1.87 to 1.57 kcal./mole. These figures represent the variation of $U_{o_{diff}}$ and Q_{diff} from $\theta = 0$ to $\theta = 0.3$. Now if we consider the determined energy site distribution for Sample B1, we see that the mean adsorptive potential was 1.21 kcal./mole. It is now obvious that the adsorptive potential of liquid argon is greater than the adsorptive potential of about two-thirds of the cellulose surface. This confirms the hypothesis of Ross and Olivier (9) that for surfaces exhibiting low and heterogeneous adsorptive potentials, multilayer buildup proceeds on the more energetic surface patches, while that part of the surface with U_o values less than that of the liquid adsorbate remains sparsely occupied.

TABLE X

EXPERIMENTAL DIFFERENTIAL HEATS OF ADSORPTION

θ	Q_{diff}, kcal./mole
0.10	2.15
0.15	2.00
0.20	1.90
0.25	1.86
0.30	1.78
0.35	1.76
0.40	1.72

Figure 22 clearly demonstrates the relationship between the energy site distribution curve of Sample B1 and the adsorptive potential of liquid argon, as discussed in the preceding paragraph.

It should be emphasized that a linear B.E.T. plot is no justification for the applicability or accuracy of the theory. In the present study, linear B.E.T. plots were obtained for all adsorbent studied. It, therefore, appears that for low potential surfaces (and they are quite numerous) the B.E.T. theory supplies only an estimate of the area of the surface having an adsorptive potential greater than that of the liquid adsorbate.

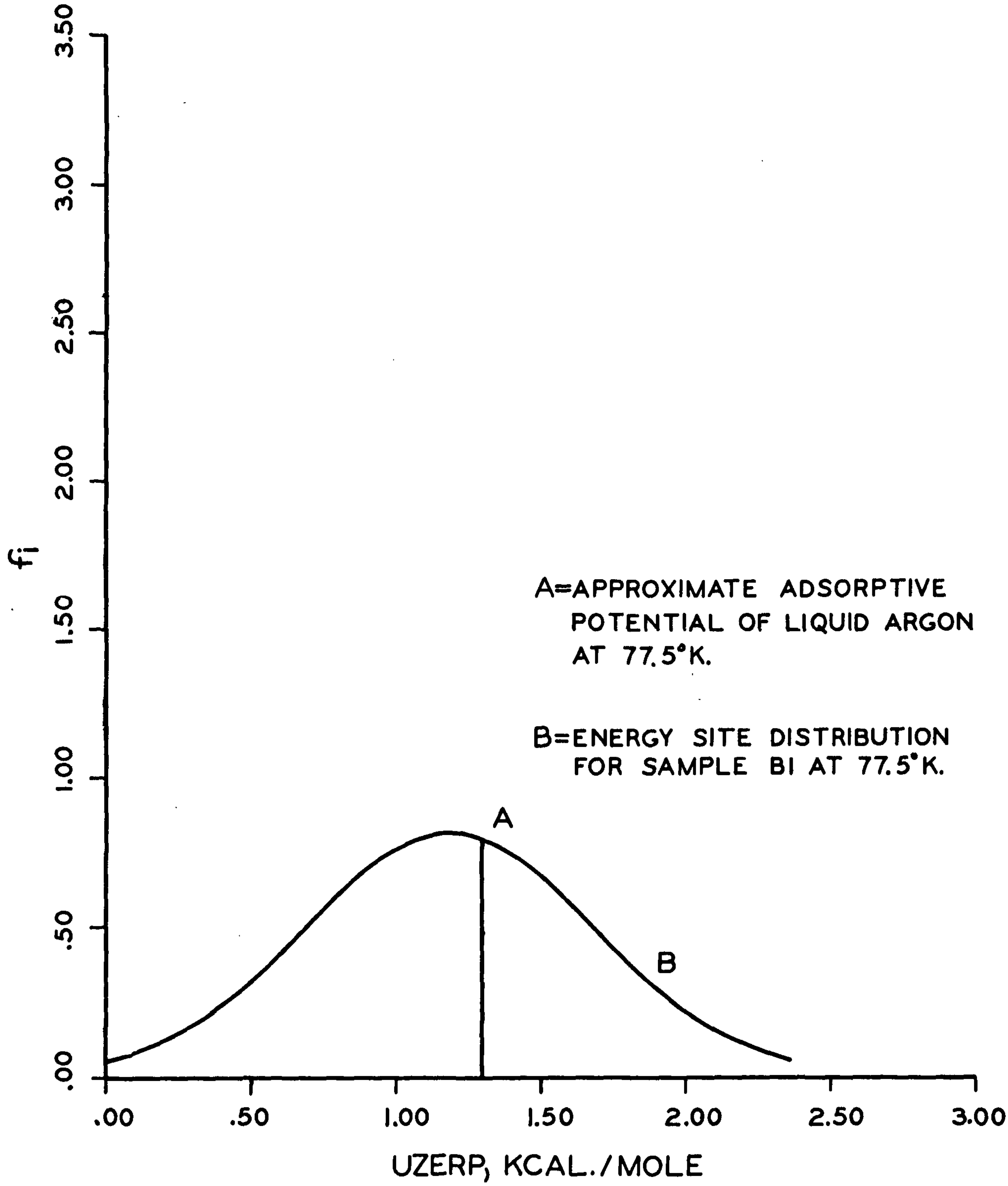

Figure 22. Relationship Between the Energy Site Distribution of Cellulose Sample B1 and the Adsorptive Potential of Liquid Argon at 77.5°K

ENTROPY OF THE ADSORBED STATE

It is the opinion of Gregg and Sing (16) that entropy calculations are of limited value in relation to the determination of monolayer capacity. He arrived at this conclusion following a discussion of the literature related to the calculation of the entropy of the adsorbed phase. Drain and Morrison (7) obtained a minimum in the plot of molar entropy of the adsorbed phase *vs.* volume adsorbed in the region of the B.E.T. v_m for argon on rutile. This result has been observed for at least five other adsorption systems, as discussed by Gregg and Sing (16).

Ross and Olivier (9) characterized rutile as exhibiting a low mean adsorptive potential and a broad range of adsorptive potentials. In light of the present work, the B.E.T. estimate of surface area for the rutile sample can be considered inaccurate. It is, therefore, unlikely that the minimum in the entropy curve of Drain and Morrison (7) actually occurred at the point of monolayer completion. It is more likely that the entropy minimum corresponded to the degree of monolayer completion at which the adsorption sites with adsorptive potential greater than that of the liquid argon were nearly filled. This would represent the point of maximum order for the adsorbed phase. Past a surface coverage of about 0.3, the rapid increase of multilayer build-up would lead to decreased order of the adsorbed phase.

COMPARISON OF ENERGY SITE DISTRIBUTIONS OBTAINED BY THE METHOD OF ROSS AND OLIVIER WITH THOSE OBTAINED BY THE METHOD OF ADAMSON AND LING

The method of Adamson and Ling (15), unlike that of Ross and Olivier (9), permits a determination of an energy site distribution from an experimental adsorption isotherm without the necessity of placing restrictions on the shape of the distribution (e.g., Gaussian). However, the Adamson and Ling method does require a previous estimate of the monolayer capacity. Adamson and Ling (15) used B.E.T. v_m estimates.

According to their theory, it is possible to define $\underline{F}$, the integral energy site distribution, as

$$F = \int f(Q)dQ \qquad (36)$$

then

$$\Theta(p,T) = \int_0^1 \theta(Q,p,T)dF. \qquad (37)$$

Then by choosing any local isotherm equation (which contains a term related to $\underline{Q}$, the adsorbent-adsorbate interaction energy) it is possible to obtain $\underline{F}$ by a method of successive approximations. Adamson and Ling (15) chose the Langmuir equation

$$\theta = \frac{bp}{1+bp} \qquad (38)$$

as the local isotherm equation, where

$$b = b_o \exp^{(Q/RT)} \qquad (39)$$

and $\underline{b_o}$ is a constant.

Adamson and Ling (15) analysis was carried out for argon adsorption on Sample B1 at 77.5°K, using the Langmuir model and B.E.T. $\underline{v_m}$ estimate. The resulting energy site distribution curve is shown in Fig. 23. It can be seen that the distribution obtained is markedly narrower than the corresponding Ross and Olivier (9) distribution (Fig. 7). This result may be attributed to one or more of the following:

1. Corrections for multilayer adsorption were not completely accounted for.
2. The B.E.T. $\underline{v_m}$ estimate was grossly in error.
3. The Langmuir model of localized adsorption without lateral interaction was not applicable.

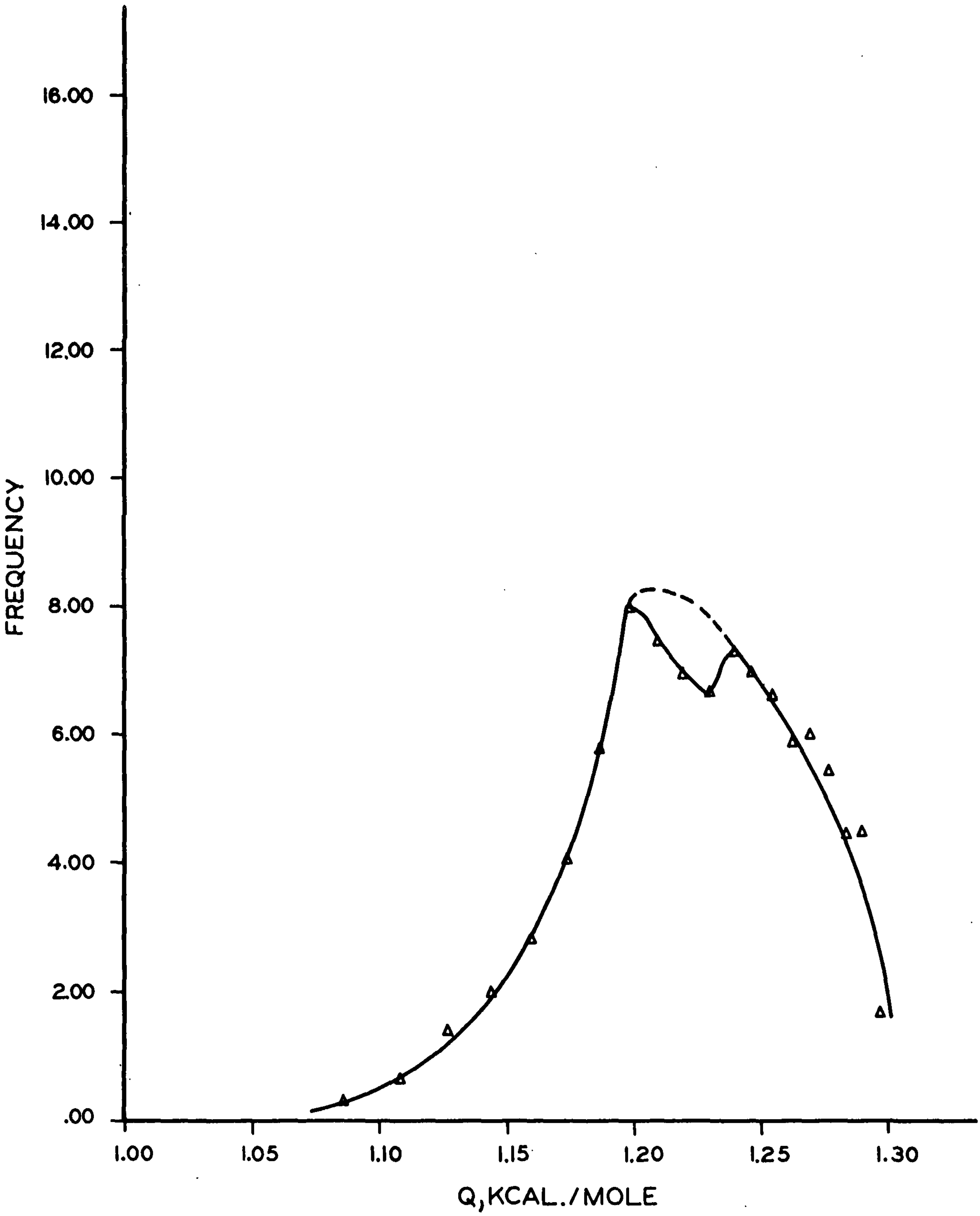

Figure 23. Adamson and Ling Energy Site Distribution for Argon Adsorption on Sample B1 at 77.5°K

Based on the above results, it appeared that a more fruitful approach would be a combination of the Adamson and Ling (15) general procedure with the Hill de Boer equation as the local isotherm function utilizing a Ross and Olivier (9) V_β estimate. For the initial step function approximation, the Hill de Boer equation [Equation (14)] was solved for p/K' when $\theta_i = 0.50$. A value of $p/K' = 0.1053$ was obtained. Then a plot of θ_{exp} vs. log (1/10.53p) was constructed as a first approximation of the F vs. $1/K$ distribution. Difficulties were encountered at this point. Since multilayer adsorption commenced at about $\Theta = 0.3$, data collected at pressures greater than 40 mm. Hg could not be used for the analysis. The data proved insufficient to produce a closed distribution since values were not available at $\Theta > 0.3$. To remedy this, it was initially thought that the experimental curve could be extended to cover higher Θ and pressure values by supplementing experimental data with the corresponding higher Θ and pressure values of the matching theoretical Ross and Olivier monolayer isotherm. This indeed permitted the determination of a complete distribution curve. However, it was necessarily identical [by Equation (1)] to the Ross and Olivier theory curve. All that was accomplished by the above attempts was an exercise in obtaining $f(U_o)$ by two mathematical means. The method of Ross and Olivier (9) is more direct, simpler, and requires neither a previous estimate of the monolayer capacity nor a step function approximation.

APPLICATIONS OF RESULTS

BOND STRENGTH AND BONDED AREA VALUES FOR PAPER

Stone (43) determined bond strength values of several pulps by making use of gas adsorption (B.E.T.) and optical scattering measurements before and after straining. The ratio of (B.E.T. surface area/optical scattering coefficient) varied from pulp to pulp. Table XI lists the ratios of surface area/optical scattering coefficient for alkali-extracted spruce sulfite and bleached spruce kraft pulps. It is unfortunate that Stone's calculations were based on only single scattering coefficient measurements. $\underline{R}_1$ represents the ratio (B.E.T. area/optical scattering coefficient), while $\underline{R}_2$ represents the ratio (Ross and Olivier area/optical scattering coefficient).

TABLE XI

RATIO OF SURFACE AREA/OPTICAL SCATTERING COEFFICIENT

Type of Pulp	Percent Hemicellulose	$\underline{R}_1$	$\underline{R}_2$
Alkali extracted spruce sulfite	4.9	26.5	77.5[a]
Bleached spruce kraft	15.7	19.8	77.3[b]

[a]Calculated on assumption that $\sum_{R.O.}/\sum_{B.E.T.}$ ratio of alkali extracted spruce sulfite was identical to that for purified cotton, i.e., about 2.90.

[b]Calculated on assumption that $\sum_{R.O.}/\sum_{B.E.T.}$ ratio of bleached spruce kraft pulp (total hemicellulose content of 15.7%) was identical to that of incense cedar holocellulose (total hemicellulose content of 13.7%). The ratio $\sum_{R.O.}/\sum_{B.E.T.}$ was 3.91 for this case.

It is interesting to note that a significant change occurred in the B.E.T. based ratios while the ratios calculated from estimated Ross and Olivier (9) areas remained unchanged. The comparison of B.E.T. based quantities for samples of different mean adsorptive potential can easily give erroneous results.

It should be emphasized that the relative accuracy of B.E.T. area estimates is a function of the chemical and physical makeup of the sample in question. Unless the samples in question possess identical energy site distributions, comparisons of B.E.T. based quantities are not valid, even on a relative basis. This is certainly applicable to the determination of such quantities as surface area, bonded area, and bond strength values for different pulps.

Since Ross and Olivier (9) area estimates are not a function of the mean adsorptive potential of the sample, they are better suited for the determination of quantities dependent on gas adsorption measurements.

Use of Ross and Olivier area estimates would lead to absolute bonded area estimates about three times greater than those now obtained with B.E.T. areas.

SURFACE AREA DETERMINATIONS

From consideration of previous discussions, it is obvious that the B.E.T. theory is not suitable for accurate surface area determinations of adsorbents which exhibit low mean adsorptive potentials in conjunction with broad energy site distributions.

Surface area determinations from adsorption measurements made with a gas flow sorptometer and based on a standard sample area (e.g., titanium dioxide) are also subject to the error introduced by the B.E.T. theory. For example, relative comparisons of surface area estimates may be in error when the samples exhibit different energy site distributions. Even when a Ross and Olivier (9) area is used as a standard in conjunction with sorptometer measurements, one should proceed with caution. The area under a sorptometer curve is proportional to the volume adsorbed at a given partial pressure. For the case where the sample in question possesses an energy site distribution different from that of the standard, isotherm plots of Θ vs. p/p_o will not have the same shape. Therefore, different surface coverages exist at the same p/p_o value, and the surface area of the sample cannot be based on that of the standard.

To make use of a gas sorptometer for Ross and Olivier (9) type analysis would require the use of several mixtures of adsorbate to produce different p/p_o values. Then, complete isotherm determination would be possible, and analysis by the Ross and Olivier method could be achieved directly.

SUGGESTIONS FOR FUTURE WORK

1. The evaluation of the surface electric field strength *F* of cellulose would be most valuable for further application of Ross and Olivier (*9*) type analysis to the surface of cellulose. When an estimate of *F* has been obtained, one can calculate the true $2\alpha/RT\beta$ level for matching experimental to theoretical isotherms by taking into account the polarization of the adsorbate. An estimate of *F* could be obtained by a calorimetric study of the heats of wetting of cellulose in a series of liquids according to the procedure of Chessick, *et al.* (*44*) and Zettlemoyer and Narayan (*45*).

2. Once the magnitude of *F* has been determined, analyses involving more complex adsorbate molecules could be attempted. The determination of the characteristics of adsorption of a polar molecule such as methanol would be of interest.

3. Once the above two studies have been completed, analyses of the complex problem of water adsorption on cellulose could be attempted on a fundamental thermodynamic basis.

CONCLUSIONS

It was demonstrated that the theory of Ross and Olivier (9) was applicable for the determination of the energy site distribution of the surface of cellulose.

Cotton cellulose, regardless of available surface area, was characterized as exhibiting a very broad range of adsorptive potentials with a low mean adsorptive potential.

For all adsorbent samples studied, marked discrepancies were observed between B.E.T. and Ross and Olivier (9) estimates of surface area. The B.E.T. surface area estimates were shown to be grossly in error when comparisons of geometric area measurements were made with B.E.T. gas adsorption areas. However, the theory of Ross and Olivier consistently predicted reasonable surface area estimates.

The B.E.T. theory is not valid for obtaining surface area estimates for samples exhibiting low mean adsorptive potentials and heterogeneous energy site distributions. "Low mean adsorptive potentials" may be considered present if a significant part of the surface exhibits adsorptive potentials less than that of the liquid adsorbate.

The construction of a linear B.E.T. plot from adsorption data was shown to be an insufficient criterion for obtaining valid gas adsorption surface area estimates.

The ratio of $\Sigma_{R.O.}/\Sigma_{B.E.T.}$ varied from 2.25 to 3.97 and was shown to be dependent upon the mean adsorptive potential, $\underline{U}'_o$, of the sample. The lower the value of $\underline{U}'_o$, the greater the ratio $\Sigma_{R.O.}/\Sigma_{B.E.T.}$.

It was concluded that for samples exhibiting a low mean adsorptive potential, significant multilayer buildup occurred on the more energetic patches of the surface while the lower energy patches remained sparsely occupied, even at high equilibrium pressures. Calculations showed that almost two-thirds of the cellulose surface possessed adsorptive potentials less than that of liquid argon. Therefore, past a surface coverage of about 0.3, the already adsorbed argon presented a more favorable adsorptive site than the remaining bare cellulose surface.

Good agreement was obtained for surface area estimates of silver iodide by negative adsorption, capacitance, and Ross and Olivier methods. The B.E.T. area estimate for silver iodide was approximately one-third the average value of the other three methods.

It should be emphasized that the discussed inapplicability of the B.E.T. theory to low adsorptive potential adsorbents is not restricted to argon as the adsorbate. Nitrogen, krypton, and xenon can be expected to produce B.E.T. area estimates that are severely in error for adsorbents exhibiting heterogeneous energy site distributions in conjunction with a low mean adsorptive potential.

It was concluded that a minimum in the curve of entropy of the adsorbed phase *vs.* surface coverage does not necessarily occur at $\Theta = 1.0$. For low adsorptive potential adsorbents, it may occur as low as $\Theta = 0.3$.

The Ross and Olivier (9) method of obtaining an energy site distribution from an adsorption isotherm was shown to be superior to the method of Adamson and Ling (15). The Ross and Olivier method required neither an independent (B.E.T.) estimate of monolayer capacity nor a step function approximation.

The effects of structural accessibility of cellulose fibers on the determined energy site distribution were shown to be minor.

The periodate oxidation of cotton resulted in only minor changes in the determined energy site distribution. However, hydroxyethylation significantly lowered the value of the mean adsorptive potential. The presence of hemicelluloses in an incense cedar holocellulose pulp may also have had the effect of lowering the value of the mean adsorptive potential of the sample below that for cotton cellulose.

GLOSSARY OF TERMS

Wherever possible, the notation of Ross and Olivier (9) was used in this manuscript. Many of the definitions of terms listed below are identical to those given by Ross and Olivier (9) in their monograph.

A^{o}	constant defined in Equation (19)
b	Langmuir equation parameter defined in Equation (39)
b_o	constant in Equation (39)
C	constant in Equation (15)
C'	constant in Equation (6)
D	relative saturation pressure in Equation (7)
E'	Hobson's (20) adsorptive potential
E_{kin}	The difference between the total kinetic energy per mole of a molecule in the gas phase and the kinetic energy of translation and rotation per mole of a molecule in the adsorbed phase
${}_aE_o^{vib}$	average vibrational energy of adsorbed molecule
F	surface electric field
${}_aF^{vib}$	additional Gibbs free energy of the adsorbed phase due to molecular vibrations with respect to the surface
f_i	frequency of particular surface patches per unit energy interval
$f(Q)$	Adamson and Ling (15) energy site distribution function
h	Planck's constant (6.626×10^{-27} ergs/sec.)
K'	particular constant associated with the mean adsorptive potential according to Equation (18)
K_i	particular value of K for the ith patch of a heterogeneous surface
k	Boltzmannconstant (1.38×10^{-16} ergs/degrees)
M	molecular weight
N	Avogadro's number
n	normalizing factor of the Gaussian distribution

$\underline{a}\underline{P}^{ia}$	potential energy of interaction of the adsorbate
$\underline{p}$	equilibrium pressure in a system
$\underline{p}_o$	saturation pressure of the adsorbate
$\underline{Q}$	Adsorbate-adsorbent interaction energy of Adamson and Ling (15)
$\underline{q}^{st}$	isosteric heat of adsorption
$\underline{q}^{st}_{exp}$	experimental isosteric heat of adsorption
$\underline{q}^{diff}$	differential heat of adsorption
$\underline{R}$	gas constant; 1.987 cal./mole degree
ΔS^{tr}_{s}	the integral translational entropy change per mole of a gas in its standard state to a mobile adsorbed film in its standard state
$\Delta \underline{S}^{rot}$	rotational entropy change upon adsorption
$\underline{T}$	temperature in degrees Kelvin
$\underline{U}_o$	adsorptive potential of a homotattic surface
$\underline{U}'_o$	adsorptive potential of the average patch of a heterogeneous surface
$\underline{U}^{diff}_o$	differential adsorptive potential
$\underline{U}_{oi}$	adsorptive potential of the ith patch of a heterogeneous surface
$\underline{U}^{int}_o$	integral adsorptive potential
$\underline{V}_\beta$	monolayer capacity of adsorbent per gram where area occupied by each molecule equals β
$\underline{v}_m$	B.E.T. theory predicted monolayer capacity
$\underline{v}$	volume adsorbed, ml. S.T.P./g.
$\underline{Z}$	Graham's equilibrium function [Equation (7)]
α	two-dimensional van der Waals constant
β	two-dimensional van der Waals constant
γ	heterogeneity parameter in Equation (11)
$\Delta\delta_i$	fraction of surface having adsorptive potentials between $\underline{U}_{oi}$ and $\underline{U}_{oi} + \underline{U}_o$
Θ	overall monolayer completion fraction
$\Theta(\underline{p},\underline{T})$	overall monolayer completion fraction

$\Theta(\underline{p})_{\underline{T}}$	overall monolayer completion fraction
$\theta_{\underline{s}}$	standard state of the surface phase, taken so that the average intermolecular separation would be the same in both the gas and adsorbed phases at $0^{\circ}C$.
$\theta_{\underline{i}}$	fraction of the $\underline{i}$th patch of the adsorbent surface covered by the adsorbate
$\theta(\underline{p},\underline{U}_o)$	local isotherm function
$\theta(\underline{p},\underline{T},\underline{U}_o)$	local isotherm function
$\theta(\underline{p},\underline{T},\underline{Q})$	local isotherm function
ν	vibrational frequency with respect to the surface acquired by a molecule on adsorption
$\phi(\underline{U}_o)$	energy site distribution function
σ_o	estimated molecular cross section of adsorbate molecule
$\sum$	surface area in $m.^2/g$.

ACKNOWLEDGMENTS

The author wishes to acknowledge the guidance and criticism extended to him by his Thesis Advisory Committee: Chairman J. W. Swanson, and Messrs. K. Ward, Jr., and R. A. Holm. The assistance of J. D. Hankey, O. A. Smith, and N. S. Thompson was also appreciated.

LITERATURE CITED

1. Stamm, A. J. Wood and cellulose science. New York, Ronald Press, 1964. 549 p.

2. Brunauer, S., Emmett, P. H., and Teller, E. J., J. Am. Chem. Soc. 60:309-19 (1938).

3. Pierce, C. J., J. Phys. Chem. 57, no. 2:149-52(Feb., 1953).

4. Haselton, W. R. An investigation of the adsorption of gases by wood and its components and of gas adsorption techniques as a means of studying the area and structure of pulp and paper. Doctor's Dissertation. Appleton, Wis., The Institute of Paper Chemistry, 1953. 172 p.

5. Rowen, J. W., and Blaine, R. L., Ind. Eng. Chem. 39:1659-63(1947).

6. Clark, D. B. Unpublished work, 1963.

7. Drain, L. E., and Morrison, J. A., Trans. Faraday Soc. 48:840-7(1952); Drain, L. E., and Morrison, J. A., Trans. Faraday Soc. 49:654-73(1953).

8. Ross, S. The heterogeneity of solid substrates. <u>In</u> Burke, Reed, and Weiss's Surfaces and interfaces. I. p. 169-96. Syracuse University Press, Syracuse, New York, 1967.

9. Ross, S., and Olivier, J. P. On physical adsorption. New York, Interscience, 1964. 401 p.

10. Chessick, J. J., and Zettlemoyer, A. C., J. Phys. Chem. 62:1217-19(1958).

11. Young, G. J., and Healey, F. H., J. Phys. Chem. 58:885(1954).

12. Sips, R., J. Chem. Phys. 16:490(1948).

13. Honig, J. M., and Reyerson, L. H., J. Phys. Chem. 46:140(1952).

14. Harkins, W. D., and Stearns, R. S., J. Phys. Chem. 58:292(1954).

15. Adamson, A. W., and Ling, I. Advances in Chemistry Series No. 33. Washington, D. C., Am. Chem. Soc., 1961. 51 p.

16. Gregg, S. J., and Sing, K. S. W. Adsorption, surface area, and porosity. New York, Academic, 1967. 371 p.

17. Ross, S., and Winkler, W., J. Am. Chem. Soc. 76:2637(1954).

18. Hsieh, P. Y., J. Phys. Chem. 68:1068(1964).

19. Adamson, A. W., Ling, I., Dormant, L., and Orem, M., J. Colloid Interface Sci. 21:445-57(1966).

20. Hobson, J. P., Can. J. Phys. 43:1941-50(1965).

21. Graham, D., J. Phys. Chem. 57:665(1953).

22. Ross, S., and Pultz, W. W., J. Colloid Sci. 13:397(1958).

23. Cochrane, H., Walker, P. L., Diethorn, W. S., and Friedman, H. C. Xenon adsorption on graphitized carbon blacks over a wide coverage range. 41st National Colloid Symposium, Buffalo, New York, June, 1967.

24. Ehrlich, G., and Hudda, F. G., J. Chem. Phys. 30:493(1959).

25. Hill, T. L., J. Chem. Phys. 14, no. 2:441-53(1946).

26. Sommers, R. A. A surface-area study of cotton dried from liquid carbon dioxide at zero surface tension. Doctor's Dissertation. Appleton, Wis., The Institute of Paper Chemistry, June, 1963. 157 p.

27. Conrad, Carl M. Chemical properties of cotton cellulose. In Ward's Chemistry and chemical technology of cotton. New York, Interscience, 1955. 782 p.

28. Lund, Hakon, and Bjerrum, Jannik, Ber. 64B:210-13(1931); C.A. 25:3310.

29. Merchant, M. V. A study of certain phenomena of the liquid exchange of water-swollen cellulose fibers and their subsequent drying from hydrocarbons. Appleton, Wis., The Institute of Paper Chemistry, 1957. 124 p.

30. Nevell, T. P. Oxidation. In Whistler's Methods in carbohydrate chemistry. New York, Academic, 1963.

31. Didwania, H. P. A study of the effects of hydroxyethylation of fibers on the bonding in paper. Doctor's Dissertation. Appleton, Wis., The Institute of Paper Chemistry, June, 1968.

32. Thompson, N. S., and Kaustinen, O. A., Tappi 47:157(1964).

33. Williams, D. G., and Webb, J. T. Personal communication, 1968.

34. Deitrich, W. H. Personal communication, 1968.

35. Stamm, A. J., and Tarkow, H. J., J. Phys. Colloid Chem. 54:745-53(1950).

36. Stamm, A. J., and Hansen, L. A., Ind. Eng. Chem. 27:1480-4(1935).

37. Ingmanson, W. L., and Thode, E. F., Tappi 42:74(1959).

38. Swanson, J. W., and Steber, A. J., Tappi 42:986(1959).

39. Van den Hul, H. J. The specific surface area of silver iodide suspensions. Doctor's Dissertation. Wageningen, Netherlands, State University of Utrecht, 1966. 77 p.

40. Lijklema, J. Thesis. State University of Utrecht; work cited In Van den Hul's Doctor's Dissertation. Wageningen, Netherlands, State University of Utrecht, 1966.

41. Mackor, E. L., Rec. Trav. Chem. 70:663, 763(1950), In Van den Hul's Doctor's Dissertation. Wageningen, Netherlands, State University of Utrecht, 1966.

42. Whalen, J. W., Wade, W. H., and Porter, J. J. The surface area and structure of Teflon 6. 41st National Colloid Symposium, Buffalo, New York, June, 1967.

43. Stone, J. E., Pulp Paper Mag. Can. 64, no. 12:T528-33(1963).

44. Chessick, J. J., Zettlemoyer, A. C., Healey, F. H., and Young, G. J., Can. J. Chem. 33:251(1955).

45. Zettlemoyer, A. C., and Narayan, K. S. Heats of immersion and the vapor/solid interface. In Flood's The solid-gas interface. New York, Dekker, 1967. 1175 p.

APPENDIX

TABLE XII

ARGON ADSORPTION DATA AND SOLVENT EXCHANGE SCHEDULE FOR SAMPLE B1

(WAN dried purified cotton cellulose)

Deadspace I	0.1352
Deadspace II	0.1316
Average deadspace	0.1334

Sample weight 4.303 g.

Temperature of adsorption 77.5°K

1st Run		2nd Run	
Equilibrium Pressure, mm. Hg	Volume Adsorbed, ml. (S.T.P.)/g.	Equilibrium Pressure, mm. Hg	Volume Adsorbed, ml. (S.T.P.)/g.
0.663[a]	2.093	5.102	5.617
5.272	5.560	24.643	10.166
22.557	9.617	50.796	13.601
		72.553	16.441
		91.975	19.256
		120.369	23.410
		151.412	27.827

3rd Run		4th Run	
1.744	3.444	64.180	15.382
7.846	6.620	124.671	23.978
18.345	9.071	154.470	28.045
30.331	10.873	188.707	32.980
46.413	12.946		
66.545	15.545		

Solvent exchange schedule identical to that for Sample BO-1 (Table XVIII)

Slope of B.E.T. plot 0.02007
Intercept of B.E.T. plot 0.00077
Correlation coefficient of least squares regression line 0.9999

[a]The adsorption data tabulated throughout the Appendix is in the form of a particular format for computer output. It is felt that the measurements are statistically significant to three figures.

TABLE XIII

ARGON ADSORPTION DATA FOR SAMPLE B1

(WAN dried purified cotton cellulose)

Deadspace I	0.1172 ml./mm.
Deadspace II	0.1168 ml./mm.
Average deadspace	0.1170 ml./mm.

Sample weight 4.303 g.

Temperature of adsorption 90.1°K

1st Run		2nd Run	
Equilibrium Pressure, mm. Hg	Volume Adsorbed, ml. (S.T.P.)/g.	Equilibrium Pressure, mm. Hg	Volume Adsorbed, ml. (S.T.P.)/g.
10.412	2.480	3.570	1.386
24.422	3.827	17.538	3.175
42.194	5.002	31.745	4.284
80.752	6.618	57.154	5.640
214.174	9.832	113.963	7.527
420.026	14.169	170.215	8.864
		255.232	10.610

3rd Run

23.113	3.752
96.742	7.130
117.556	9.092
282.526	11.620
386.440	13.558
499.830	16.223

Slope of B.E.T. plot[a] 0.0239
Intercept of B.E.T. plot 0.0011
Correlation coefficient for least squares regression line 0.9988

[a]B.E.T. calculations carried out theoretical value of $\underline{P_o}$ for argon at 90.1°K (46) since apparatus was not capable of measuring this high a $\underline{P_o}$ value (1045 mm. Hg).

TABLE XIV

ARGON ADSORPTION DATA AND SOLVENT EXCHANGE CONDITIONS FOR SAMPLE B3

(WAN dried purified cotton cellulose)

Deadspace I	0.1281 ml./mm.
Deadspace II	0.1310 ml./mm.
Deadspace III	0.1322 ml./mm.
Average deadspace	0.1304 ml./mm.

Sample weight 4.1849 g.

Temperature of adsorption 77.5°K

1st Run		2nd Run	
Equilibrium Pressure, mm. Hg	Volume Adsorbed, ml. (S.T.P.)/g.	Equilibrium Pressure, mm. Hg	Volume Adsorbed, ml. (S.T.P.)/g.
0.012	0.119	0.640	2.277
0.064	0.700	3.029	4.608
0.309	1.546	6.979	6.563
1.355	3.164	13.562	8.444
4.191	5.382	20.916	9.850
8.595	7.303	31.074	11.403
14.576	8.911		
21.116	10.182		

Displacement Size, cc.	Material	Exchanges	Minimum Contact Time, hr.	min.
85	Methanol	B3-1 to B3-15		10
500	Dried methanol	B3-16	2	0
85	Dried methanol	B3-17 to B3-31		30
400	Dried pentane	B3-32	2	0

Slope of B.E.T. plot 0.0209
Intercept of B.E.T. plot 0.00062
Correlation coefficient for least squares regression line 0.999

TABLE XV

ARGON ADSORPTION DATA FOR SAMPLE B3-H50

(Sample B3, humidified at 50% R.H. and redried)

Deadspace I	0.1309 ml./mm.
Deadspace II	0.1306 ml./mm.
Average deadspace	0.1308 ml./mm.

Sample weight 4.1849 g.

Temperature of adsorption 77.5°K

Equilibrium Pressure, mm. Hg	Volume Adsorbed, ml. (S.T.P.)/g.
1.608	3.053
5.284	5.221
11.303	7.128
20.753	8.892
30.994	10.292
39.907	11.390

Slope of B.E.T. plot 0.02089

Intercept of B.E.T. plot 0.00062

Correlation coefficient for least squares regression line 0.9999

TABLE XVI

ARGON ADSORPTION DATA FOR SAMPLE B3-H86

(Sample B3, humidified at 86.5% R.H. and redried)

Deadspace I	0.1294 ml./mm.
Deadspace II	0.1290 ml./mm.
Average deadspace	0.1292 ml./mm.

Sample weight 4.1849 g.

Temperature of adsorption 77.5°K

Equilibrium Pressure, mm. Hg	Volume Adsorbed, ml. (S.T.P.)/g.
0.324	0.576
3.592	1.688
9.811	3.184
17.974	4.505
27.662	5.602
44.297	7.179
56.387	8.252
97.802	12.545
134.894	17.298

Slope of B.E.T. plot 0.03216
Intercept of B.E.T. plot 0.00242
Correlation coefficient for least squares regression line 0.9999

TABLE XVII

ARGON ADSORPTION DATA FOR SAMPLE B4

(Water dried purified cotton cellulose)

Deadspace I	0.1338 ml./mm.
Deadspace II	0.1334 ml./mm.
Average deadspace	0.1336 ml./mm.

Sample weight 3.1342 g.

Temperature of adsorption 77.5°K

1st Run Equilibrium Pressure, mm. Hg	1st Run Volume Adsorbed, ml. (S.T.P.)/g.	2nd Run Equilibrium Pressure, mm. Hg	2nd Run Volume Adsorbed, ml. (S.T.P.)/g.
2.561	0.041	2.469	0.030
8.957	0.074	5.686	0.040
18.821	0.101	12.193	0.072
31.575	0.124	29.046	0.115
43.928	0.132	39.270	0.138
75.682	0.175	51.050	0.157
130.665	0.239	66.926	0.172

3rd Run Pressure	3rd Run Volume	4th Run Pressure	4th Run Volume
7.088	0.066	2.645	0.035
15.202	0.092	6.142	0.058
27.132	0.106	12.646	0.085
41.465	0.118	27.111	0.117
52.978	0.124		
75.621	0.134		
108.924	0.164		

5th Run Pressure	5th Run Volume	6th Run Pressure	6th Run Volume
3.007	0.038	14.289	0.082
7.660	0.062	35.000	0.125
18.435	0.096	55.594	0.131
32.680	0.130		

7th Run Pressure	7th Run Volume
25.478	0.102
43.800	0.116
70.492	0.134

Slope of B.E.T. plot 2.15
Intercept of B.E.T. plot 0.0717
Correlation coefficient for least squares regression line 0.966

TABLE XVIII

ARGON ADSORPTION DATA, SOLVENT EXCHANGE CONDITIONS, AND DEGREE OF OXIDATION OF SAMPLE BO-1

(Periodate oxidized purified WAN dried cotton cellulose)

Deadspace I	0.1316 ml./mm.
Deadspace II	0.1312 ml./mm.
Average deadspace	0.1314 ml./mm.

Sample weight 4.5069 g.

Temperature of adsorption 77.5°K

1st Run		2nd Run	
Equilibrium Pressure, mm. Hg	Volume Adsorbed, ml. (S.T.P.)/g.	Equilibrium Pressure, mm. Hg	Volume Adsorbed, ml. (S.T.P.)/g.
5.260	1.689	0.049	0.203
22.109	2.754	0.247	0.483
35.219	3.271	1.426	0.957
65.728	4.213	4.681	1.624
117.841	6.680	8.159	1.997
147.441	9.096	13.440	2.371

3rd Run	
0.235	0.481
1.513	1.048
11.500	2.266
33.751	3.256
69.692	4.450
95.913	5.532
131.362	7.810

Displacement Size, cc.	Material	Exchanges	Minimum Contact Time, hr.	min.
50	Methanol	BO-1-1		10
40	Methanol	BO-1-2 to BO-1-11		10
40	Dried methanol	BO-1-12 to BO-1-15		10
40	Dried pentane	BO-1-16 to BO-1-25		10

Slope of B.E.T. plot 0.0728
Intercept of B.E.T. plot 0.00184
Confidence coefficient for least squares regression line 0.9998

Degree of oxidation 0.136 g. oxygen consumed/g. oxidized cellulose

TABLE XIX

ARGON ADSORPTION DATA OF SAMPLE BHYD-1

(Hydroxyethylated cotton combers)

Deadspace I	0.2316 ml./mm.
Deadspace II	0.2325 ml./mm.
Average deadspace	0.2321 ml./mm.

Sample weight 12.5755 g.

Temperature of adsorption 77.5°K

1st Run		2nd Run	
Equilibrium Pressure, mm. Hg	Volume Adsorbed, ml. (S.T.P.)/g.	Equilibrium Pressure, mm. Hg	Volume Adsorbed, ml. (S.T.P.)/g.
8.963	0.706	11.073	0.063
18.750	1.050	22.118	0.087
35.138	1.325	31.887	0.103
52.142	1.531	44.102	0.117
		61.503	0.136

Slope of B.E.T. plot 0.7556
Intercept of B.E.T. plot 0.0291
Correlation coefficient of least squares regression line 0.9992

TABLE XX

ARGON ADSORPTION DATA AND RESULTS OF CHEMICAL ANALYSIS
OF SAMPLE BHOLO-1

(Incense cedar chlorite holocellulose)

Deadspace I	0.1974 ml./mm.
Deadspace II	0.1974 ml./mm.
Average deadspace	0.1974 ml./mm.

Sample weight 13.7010 g.

Temperature of adsorption 77.5°K

1st Run		2nd Run	
Equilibrium Pressure, mm. Hg	Volume Adsorbed, ml. (S.T.P.)/g.	Equilibrium Pressure, mm. Hg	Volume Adsorbed, ml. (S.T.P.)/g.
8.180	0.010	5.522	0.007
15.129	0.017	11.408	0.012
24.070	0.023	29.963	0.020
34.717	0.031	39.312	0.028
42.110	0.032	53.636	0.032
62.033	0.044		

Slope of B.E.T. plot 1.82
Intercept of B.E.T. plot 0.249
Correlation coefficient for least squares regression line 0.921

	Incense Cedar Chlorite Holocellulose		
	Test 1	Test 2	Average
Glucan, %	63.74	65.27	64.5
Xylan, %	6.81	7.06	6.9
Mannan, %	6.73	6.84	6.8
Araban, %			None[a]
Galactan, %	1.10	0.96	1.0

[a]Limit of detection = 0.5%.

Basis of report: Moisture free (dried under vacuum over P_2O_5).

Method: Saeman, J. F., Moore, W. E., Mitchell, R. L., and Millett, M. A., Tappi 37:336(1954).

TABLE XXI

ARGON ADSORPTION DATA AND GEOMETRIC AREA MEASUREMENTS
FOR SAMPLE B5-RAY

(Viscose rayon)

Deadspace I	0.1991 ml./mm.
Deadspace II	0.1977 ml./mm.
Average deadspace	0.1984 ml./mm.

Sample weight 9.5787 g.

Temperature of adsorption 77.5°K

1st Run		2nd Run	
Equilibrium Pressure, mm. Hg	Volume Adsorbed, ml. (S.T.P.)/g.	Equilibrium Pressure, mm. Hg	Volume Adsorbed, ml. (S.T.P.)/g.
10.452	0.029	10.737	0.032
20.484	0.038	20.389	0.042
29.991	0.046	30.832	0.044
		40.728	0.052
		51.779	0.057
		69.981	0.062

3rd Run

6.351	0.021
16.378	0.039
26.975	0.049
36.700	0.053
45.355	0.057

Slope of B.E.T. plot 2.14
Intercept of B.E.T. plot 0.072
Confidence coefficient for least squares regression line 0.989

Fibers were embedded in celloidin, mounted in mineral oil for optical tracings of projected fiber images (750X).

Mean rayon fiber circumference = 5.72×10^{-3} cm. $\pm 0.16 \times 10^{-3}$ cm. at 95% confidence limits based on 77 observations.

For 1.5 denier rayon, we have 6000 m./g.

Geometric surface area = 6000 m./g. $\times 5.72 \times 10^{-5}$ m. = <u>0.342 m.^{2}/g.</u>

TABLE XXI (Continued)

ARGON ADSORPTION DATA AND GEOMETRIC AREA MEASUREMENTS
FOR SAMPLE B5-RAY

(Viscose rayon)

For a check on the denier value, the length of fiber per gram may be calculated once the fiber density and average fiber cross section are known. From 77 planimetered areas of projected fiber cross sections, the mean cross-sectional area was determined to be 11.8×10^{-7} cm.^{2} $\pm$ 0.36×10^{-7} cm. at the 95% confidence level. Using a value of 1.55 g./cm.^{3} which represents the helium density of rayon, a length of 5470 m./g. was determined for the sample. A low value such as obtained would be expected, since estimates of fiber perimeters were low due to difficulties involved in interpreting projected images (e.g., depth of flutes, surface roughness).

Magnification = (750X)(7.45X)

TABLE XXII

ARGON ADSORPTION DATA AND GEOMETRIC AREA MEASUREMENTS
FOR SAMPLE B6-RAY

(High tenacity viscose rayon)

Deadspace I	0.2260 ml./mm.
Deadspace II	0.2266 ml./mm.
Average deadspace	0.2263 ml./mm.

Sample weight 11.737 g.

Temperature of adsorption 77.5°K

1st Run		2nd Run	
Equilibrium Pressure, mm. Hg	Volume Adsorbed, ml. (S.T.P.)/g.	Equilibrium Pressure, mm. Hg	Volume Adsorbed, ml. (S.T.P.)/g.
6.786	0.022	5.102	0.020
15.672	0.037	14.849	0.037
27.909	0.050	24.708	0.044
38.131	0.054	41.942	0.053
47.968	0.058	54.346	0.058
56.573	0.065	69.028	0.072

Slope of B.E.T. plot 1.683
Intercept of B.E.T. plot 0.0623
Correlation coefficient for least squares regression line 0.995

Fibers were embedded in celloidin, mounted in mineral oil for optical tracings of projected fiber images (750X).

Mean rayon fiber circumference = 4.21×10^{-3} cm. $\pm$ 0.06×10^{-3} cm. at 95% confidence limits based on 48 observations.

For 1.5 denier rayon, we have 6000 m./g.

Geometric surface area = 6000 m./g. x 4.21×10^{-5} m. = $\underline{0.252 \text{ m.}^2/\text{g.}}$

Magnification = (8.82X)(750X)

TABLE XXIII

ARGON ADSORPTION DATA AND GEOMETRIC AREA MEASUREMENTS OF SAMPLE $BTiO_2$-1

(Anatase)

Deadspace I	0.007774 ml./mm.
Deadspace II	0.008286 ml./mm.
Average deadspace	0.00803 ml./mm.

Sample weight 1.0517 g.

Temperature of adsorption 77.5°K

1st Run: Equilibrium Pressure, mm. Hg	1st Run: Volume Adsorbed, ml. (S.T.P.)/g.	2nd Run: Equilibrium Pressure, mm. Hg	2nd Run: Volume Adsorbed, ml. (S.T.P.)/g.
1.521	0.569	2.730	1.093
3.055	1.289	10.257	1.683
74.468	3.192	23.942	2.103
		42.815	2.440
		59.579	2.706

3rd Run

3.268	1.223
14.558	1.788
32.856	2.181
43.504	2.352

Slope of B.E.T. plot 0.483
Intercept of B.E.T. plot 0.0056
Correlation coefficient of least squares regression line 0.9994

Geometric area = 12.73 $m.^2/g.$ (33)